

CONFIDENTIAL

Copy 455
RM L56B24

NACA

CASE FILE
COPY

RESEARCH MEMORANDUM

AERODYNAMIC CHARACTERISTICS OF A 6-PERCENT-THICK
SYMMETRICAL CIRCULAR-ARC AIRFOIL HAVING A
30-PERCENT-CHORD TRAILING-EDGE FLAP AT
A MACH NUMBER OF 6.9

By Herbert W. Ridyard and David E. Fetterman, ^{NO. 7} WHL

Langley Aeronautical Laboratory
Langley Field, Va.

CLASSIFIED DOCUMENT

This material contains information affecting the National Defense of the United States within the meaning of the espionage laws, Title 18, U.S.C., Secs. 793 and 794, the transmission or revelation of which in any manner to an unauthorized person is prohibited by law.

CLASSIFICATION CHANGED TO UNCLASSIFIED
AUTHORITY: NASA PUBLICATIONS ANNOUNCEMENT
EFFECTIVE DATE: MAY 29, 1959

NATIONAL ADVISORY COMMITTEE
FOR AERONAUTICS

WASHINGTON

June 5, 1956

CONFIDENTIAL

NATIONAL ADVISORY COMMITTEE FOR AERONAUTICS

RESEARCH MEMORANDUM

AERODYNAMIC CHARACTERISTICS OF A 6-PERCENT-THICK
SYMMETRICAL CIRCULAR-ARC AIRFOIL HAVING A
30-PERCENT-CHORD TRAILING-EDGE FLAP AT
A MACH NUMBER OF 6.9

By Herbert W. Ridyard and David E. Fetterman, Jr.

SUMMARY

An investigation, including pressure distributions and schlieren flow photographs, has been made of the flow characteristics over a 6-percent-thick symmetrical circular-arc airfoil section with a 30-percent-chord trailing-edge flap at a Mach number of 6.90 and a Reynolds number of 1.65×10^6 . The model was tested over an angle-of-attack range of 0° to 16° and a flap-deflection range of -16° to 16° . The experimental pressure distributions are in good agreement with the results of shock-expansion theory except in the regions of flow separation resulting from shock-boundary-layer interaction. Even though differences occur between the theoretical and the experimental pressure distributions, the results of shock-expansion theory adequately predict the integrated experimental aerodynamic characteristics except in some cases for large flap deflections. The flap was continuously effective throughout the test angle range.

INTRODUCTION

A program has been undertaken at the Langley Aeronautical Laboratory to determine the flow characteristics of rectangular wings having 6-percent-thick and 9-percent-thick symmetrical circular-arc airfoil sections and trailing-edge flaps. This program was initiated because most of the previous work dealing with the aerodynamic characteristics of controls at supersonic speeds had been limited to three-dimensional control surfaces and techniques that determine only the overall characteristics of the control surfaces and gave little or no insight into the reasons for the discrepancies, which had been found to exist, between theoretical and experimental results.

The first comprehensive investigation to discover some of the reasons for these discrepancies was made at Mach numbers of 1.62, 1.93, and 2.40 and a Reynolds number of 1.07×10^6 and was reported in references 1 and 2. The results of these tests showed that laminar separation on the low-pressure side of the flap and in the vicinity of the hinge line on that side of the airfoil which is adjacent to the high-pressure side of the flap caused regions of control ineffectiveness at low flap deflections. The tests of reference 2 showed that these separation effects were reduced or eliminated by producing transition from laminar to turbulent boundary layer with a resulting improvement in the agreement between the experimental and theoretical pressure distributions.

More recent tests (ref. 3) of these wing-flap configurations at a Mach number of 4.04 and a Reynolds number of 5.0×10^6 showed regions of flow separation similar to those previously reported in references 1 and 2 on the low-pressure side of the flap and in the vicinity of the hinge line on that side of the configuration where the low-pressure side of the wing was adjacent to the high-pressure side of the flap. However, in reference 3, flow separation was not found in the vicinity of the hinge line for the case in which the high-pressure side of the wing was adjacent to the high-pressure side of the flap as was found in references 1 and 2. Furthermore, an increase in Reynolds number from 5.0×10^6 to 8.4×10^6 decreased the extent of the areas of separated flow. For either Reynolds number, these tests at a Mach number of 4.04 showed that the wing-flap configuration was continuously effective throughout the control deflection and angle-of-attack range.

The purpose of the present investigation conducted in the Langley 11-inch hypersonic tunnel is to determine at a higher Mach number, $M = 6.9$, the effects of flow separation and shock-boundary-layer interaction on the aerodynamic characteristics of a 6-percent-thick symmetrical circular-arc airfoil having a 30-percent-chord trailing-edge flap. These effects were investigated at a Reynolds number of 1.65×10^6 by obtaining two-dimensional pressure distributions and schlieren flow photographs through an angle-of-attack range from 0° to 16° and a flap-deflection range from -16° to 16° .

The effect of Mach number on the theoretical and experimental aerodynamic characteristics is presented as a brief summary of the available data on these wing-flap configurations.

SYMBOLS

p_L local static pressure on airfoil

p stream static pressure

- M stream Mach number
- R Reynolds number, based on airfoil chord length
- γ ratio of specific heats for air, 1.4
- q stream dynamic pressure, $\frac{1}{2} \rho M^2$
- P pressure coefficient, $\frac{p_L - p}{q}$
- α airfoil angle of attack
- δ flap deflection relative to airfoil chord, positive downward
- c chord of airfoil
- c_f chord of flap
- x/c distance from leading edge in chords
- l section lift
- d section pressure drag
- $m_{.5}$ section pitching moment about midchord (positive when it tends to rotate the leading edge upward)
- h flap section hinge moment (positive when it tends to deflect the flap downward)
- c_l section lift coefficient, l/qc
- c_d section drag coefficient, d/qc
- c_{dp} minimum section pressure drag coefficient
- c_l/c_d section lift-drag ratio
- c_m section pitching-moment coefficient about midchord, $m_{.5}/qc^2$
- c_h section flap hinge-moment coefficient, h/qc_f^2
- c_{la} variation of section lift coefficient with angle of attack

- $c_{m\alpha}$ variation of section pitching-moment coefficient with angle of attack
- $c_{h\alpha}$ variation of section flap hinge-moment coefficient with angle of attack
- $c_{l\delta}$ variation of section lift coefficient with flap deflection
- $c_{lf\delta}$ variation of section flap lift coefficient with flap deflection
- $c_{m\delta}$ variation of section pitching-moment coefficient with flap deflection
- $c_{h\delta}$ variation of section flap hinge-moment coefficient with flap deflection
- $\frac{\partial c_m}{\partial c_l}$ variation of section pitching-moment coefficient with section lift coefficient
- $\frac{\partial \alpha}{\partial \delta}$ flap effectiveness factor, $\frac{\partial c_l / \partial \delta}{\partial c_l / \partial \alpha}$
- $(\frac{x}{c})_{cp}$ distance of airfoil center of pressure from leading edge of airfoil in chords, positive downstream

APPARATUS AND TESTS

Wind Tunnel

The tests were conducted in the Langley 11-inch hypersonic wind tunnel equipped with a two-dimensional steel nozzle which is described and for which a calibration is given in reference 4. Tunnel operation is of the intermittent type with possible running times of about 1 minute with a model in the test section.

The stagnation temperature was maintained at about 675° F by means of a variable-frequency resistance-tube heater. This high stagnation temperature is used to avoid liquefaction of air in the test section (see ref. 5); however, warpage of the thin slit-like minimum of the steel nozzle due to the high thermal stresses at this section caused a small but significant variation in Mach number with time. Therefore, data were recorded at a particular time corresponding to $M = 6.9$ during each operation of the tunnel.

The absolute humidity of the air was kept less than 1.87×10^{-5} pounds of water vapor per pound of dry air for all tests.

MODEL

The basic dimensions and orifice locations of the pressure-distribution model used in these tests are shown in figure 1 and a photograph of the model and the model support, is given in figure 2. The model had a 5-inch chord, an aspect ratio of 1, a 6-percent-thick symmetrical circular-arc airfoil section, and a 30-percent-chord full-span plain trailing-edge flap. The airfoil contour was finished to within 0.001 inch of the specified ordinates and was polished smooth. The clearance between the wing and flap was 0.005 inch (0.001c). The leading- and trailing-edge angles were 13.7° .

Pressure orifices were located along the chord of the model at the midspan station which is well within the region between the Mach cones from the leading-edge tips as determined from shock-expansion theory. (See fig. 1.) Seven of the orifices were on the main wing and five on the flap. A 0.040-inch inside-diameter tube formed the pressure orifice on the upper surface of the model and projected through the undersurface (see orifice tubing detail, fig. 1) where it was connected to the 0.060-inch inside-diameter model-support tubing. At the high Mach number of this investigation, the presence of the tubing on the underside of the model should not affect the pressures on the upper surface. The pressure leads from the orifices were ducted through the model-support system to the outside of the tunnel where the pressures were measured by means of bellows-type six-cell film recording units described in reference 6.

The pressure-distribution model was also used for schlieren flow observations which were obtained simultaneously with the pressure distributions.

TESTS

The stagnation pressure for these tests was maintained at about 33 atmospheres by means of a regulating valve. This stagnation pressure together with the previously mentioned wind-tunnel conditions (stagnation temperature = $675^\circ F$ and $M = 6.9$) corresponds to a test Reynolds number of 330,000 per inch or 1.65×10^6 based on the 5-inch chord of the model. As a consequence of this relatively low test Reynolds number the boundary layer on the model was laminar; attempts to produce a turbulent boundary layer by artificial means were unsuccessful.

Angles of attack and control deflections were set to predetermined values prior to each run by means of the offset arms (shown in fig. 2), which linked the model to the sting support. Since it was possible to measure pressure distributions on only one surface of the model, the angle of attack of the wing was varied from -16° to 16° in order to obtain the pressure distributions on both the upper and lower surfaces of the wing-flap configuration. The flap was deflected from -16° to 16° for both the positive and negative angles of attack for the same reason. This method of obtaining the pressure distribution is warranted because of the symmetry of the model.

The gap between the wing and the flap was not sealed for the tests presented herein; however, a few tests were made with the gap sealed to determine the effect of the gap on the pressure distributions. A comparison of the pressure distributions with and without the gap showed a negligible effect.

PRECISION OF DATA

In the region of the test section where the models were located the Mach number variation did not exceed ± 0.06 . The free-stream Reynolds number did not vary more than $\pm 50,000$ from the value previously given. The angles of attack and flap-deflection angles were accurate to $\pm 0.2^\circ$. The estimated inaccuracy in the pressure coefficient, due to instrumentation errors and variations in the Mach number and dynamic pressure, was ± 0.01 .

The uncertainties in the aerodynamic force and moment coefficients resulting from these errors and unavoidable errors involved in the integration of the pressure distributions have been estimated and are presented as follows:

c_l	± 0.005
c_d	± 0.003
c_m	± 0.001
c_h	± 0.003

RESULTS AND DISCUSSION

Pressure Results

Pressure distributions over the wing-flap configuration for representative test-angle combinations are presented in figure 3. Schlieren flow photographs for the same test angles are divided into two parts (figs. 4 and 5); the photographs of figure 4 present the flow over the upper surface and figure 5 presents the lower surface.

Upper surface.- The experimental pressure distributions and schlieren photographs (figs. 3 and 4) indicate flow separation on the upper surface of the wing-flap configuration in the following regions for specified test angle ranges: (1) At small angles of attack (0° to 4°) and positive flap deflections, flow separation occurs over the rear portion of the flap with the separation point moving forward to the hinge line as the flap deflection increases (see figs. 4(a) and (b)). (2) At small angles of attack and negative flap deflections a region of flow separation occurs in the vicinity of the hinge line as can be seen in figures 3(b) and 4(b) ($\alpha = 4^\circ$, $\delta = -12^\circ$, -16°). These figures ($\delta = -12^\circ$, -16°) also indicate that the flow separates ahead of the hinge line, the separation point moves forward with increasingly negative flap deflections, and that reattachment of the flow occurs after the hinge line on the flap. (3) At large angles of attack (8° to 16°), the flow is separated over the entire flap and the rear portion of the wing for either positive or negative flap deflections. The first two regions of separation on the upper surface of the wing-flap as well as the forward movement of the separation point have been reported at lower Mach numbers in references 2 and 3. The third region was not found in references 2 or 3 because the limited angle-of-attack range precluded the occurrence of separation for the conditions of those tests. It is interesting to note that the local pressure coefficients corresponding to separation on the upper surface at high angles of attack are in fair agreement with the limiting pressure coefficient for separation

$$\left(P = - \frac{1}{M^2} \right) \text{ proposed in reference 7.}$$

Lower surface.- The pressure distributions and schlieren flow photographs (figs. 3 and 5) indicate two regions of flow separation on the lower surface of the wing-flap configuration as follows: (1) At positive angles of attack and high negative flap deflections, separation occurs over the rear portion of the flap. The separation point moves forward with increasing flap deflection (see figs. 3(b); $\delta = -12^\circ$, -16° and 5(b); $\delta = -8^\circ$, -16°) or with decreasing angle of attack. (2) At positive angles of attack and high positive flap deflections, local separation occurs in the vicinity of the hinge line similar to that which occurs

on the upper surface except that the increases in pressure measured at the point of separation and at the point of reattachment are relatively greater on the lower surface than on the upper surface. Both regions of flow separation on the lower surface have been noted in reference 2; however, the flow separation on the lower surface near the hinge line was not present in the tests of reference 3, probably because the Reynolds numbers of 5×10^6 to 8.4×10^6 , for the latter reference, are considerably higher than those of reference 2 ($R = 1.08 \times 10^6$) or the present tests ($R = 1.65 \times 10^6$).

Comparison with theory. - The theoretical results presented in figure 3 were determined from shock-expansion theory. On those portions of the wing-flap where flow separation does not affect the pressure distributions, theory is in good agreement with experiment; however, in general, the theoretical pressure coefficients do underestimate the experimental values. This discrepancy can be attributed to rotational flow effects which are neglected in the shock-expansion theory and to the boundary-layer-displacement effect on the surface pressures. The analysis of reference 8 indicates that the rotational flow effects would be very small for the present airfoil and test angle range and, therefore, could account for only a small part of the aforementioned discrepancy. Estimations of the boundary-layer-displacement effect have been made by the methods of references 9 and 10 which give nearly identical results. A comparison of the experimental pressure distributions and the theoretical pressure distributions with and without boundary-layer-displacement correction (using refs. 9 and 10) for $\alpha = 0^\circ$ and 8° with $\delta = 0^\circ$ is presented in figure 6. The theoretical results with boundary-layer-displacement correction are in excellent agreement with experiment where separation does not occur.

Considering once again the theoretical results of figure 3, it can be seen that in the vicinity of the hinge line, where flow separation occurs because of shock-boundary-layer interaction, the agreement between shock-expansion theory and the experimental pressure distributions is poor. Both the pressure rise at the point of separation and at the point of reattachment occur at a considerable distance from the hinge line where the calculated shock is located. This poor agreement is more pronounced for the lower surface because of the relatively higher pressures present there as compared to those of the upper surface.

The flow separation on the low-pressure side of the flap at all angles and on the rear portion of the wing upper surface at high α (figs. 3(e) and 4(e)) results in experimental pressure coefficients which are essentially the same as the theoretical results. This agreement is to be expected since at hypersonic Mach numbers, pressure coefficients are very nearly zero as long as the local pressures are less than free-stream static pressure. As a matter of fact the vacuum pressure coefficient ($p_L = 0$) for the conditions of these tests is only -0.03.

Aerodynamic Characteristics

The experimental and theoretical shock-expansion pressure distributions have been integrated to determine the section aerodynamic characteristics which are presented in figures 7 to 15; the experimental values are also presented in tabular form in table I.

Section lift coefficient.— The variations of section lift coefficient with angle of attack and flap deflection presented in figure 7 show good overall agreement between the experimental results and the results of shock expansion theory. This good agreement is indicative of the compensating nature of the large discrepancies between the theoretical and experimental pressure distributions shown in figure 3. As an example of this compensating effect, compare the variation of c_l with δ for $\alpha = 16^\circ$ in figure 7(b) with the pressure distributions for various values of δ at $\alpha = 16^\circ$ in figure 3(e). It can be seen in figure 7(b) that the difference between the experimental and theoretical curves for $\alpha = 16^\circ$ is nearly constant throughout the range of δ ; whereas, the corresponding pressure distributions (fig. 3(e)) show widely varying degrees of agreement between the experimental and theoretical pressure distributions.

The variation of the flap effectiveness factor $\partial\alpha/\partial\delta$ with section lift coefficient is presented in figure 8. In general, the theoretical results give an excellent prediction of the trends of the experimental curves except for $\delta = 16^\circ$. However, the theoretical values of $\partial\alpha/\partial\delta$ overestimate the experimental values, except for $\delta = -16^\circ$ where the agreement is excellent. This overestimation of the experimental values of $\partial\alpha/\partial\delta$ noted here arises from the difference in slopes of the theoretical and experimental curves of c_l plotted against δ (fig. 7(b)), and not from the curves of c_l plotted against α (fig. 7(a)) where the theoretical and experimental slopes are very nearly the same throughout the test range.

Section drag coefficients.— The variations of section drag coefficient with angle of attack for various values of flap-deflection angle are presented in figure 9. These coefficients are as taken from the theoretical and experimental pressure distributions and, therefore, do not include any skin-friction drag. Also, the theoretical drag coefficients do not include the displacement effects of the boundary layer on the surface pressures. The experimental results are predicted quite well by theory except for $\delta = 16^\circ$ and at low angles of attack for $\delta = -16^\circ$.

Section lift-drag ratios.— The variations of section lift-drag ratio with angle of attack for various values of flap deflection are

presented in figure 10. The high values of experimental and theoretical lift-drag ratio indicated in the figure are a result of not including skin-friction drag in the drag coefficients. The agreement between the theoretical and experimental results is reasonably good except in the vicinity of the maximum values of c_l/c_d particularly for negative flap deflections where theory greatly underestimates the experimental results because of the combination of the higher lift and lower drag values than theoretically predicted.

Section pitching-moment coefficients.- The variations of section pitching-moment coefficient with section lift coefficient are presented in figure 11. The agreement between the experimental and the theoretical results is generally good for moderate flap deflections; however, for large flap deflections the agreement is not too good because of flow separation and other effects discussed previously. Experimental values of $\partial c_m / \partial c_l$ for constant values of α at $c_m = 0$ as obtained from figure 11 are presented for various angles of attack in figure 12 and show excellent agreement with theory.

Center-of-pressure location.- The variation of the center-of-pressure location with angle of attack for various flap deflections is shown in figure 13. The experimental center-of-pressure locations agree reasonably well with the theoretical values for positive flap deflections in spite of the large flow-separation effects on the pressure distributions; at negative flap deflections, agreement between the theoretical and experimental results is poor except at high angles of attack where flow-separation effects are small.

Section flap hinge-moment coefficient.- The variations of section flap hinge-moment coefficient with angle of attack and flap deflection are presented in figure 14. The experimental values are predicted quite well by the results of shock-expansion theory except at high flap deflections. The prediction of the trends of the experimental data is good throughout the test range and no shifts or breaks in the curves are indicated. These predictions are rather surprising upon consideration of the large differences between the experimental and theoretical pressure distributions over the flap and are once again indicative of the compensating nature of these differences.

Section hinge-moment slope parameters ch_δ and ch_α for $\alpha = 0$ and $\delta = 0$, respectively, obtained from figure 14 are presented in figure 15. The theoretical results predict the trends of the experimental data very well and the agreement between the experimental and theoretical values of ch_δ is excellent; however, in the case of ch_α the agreement is only fair.

Variation of the aerodynamic characteristics with Mach number. - In order to summarize the available data on the present wing-flap configuration, figure 16 presents the variation with Mach number of the longitudinal aerodynamic slope parameters and the minimum drag coefficients for both 6- and 9-percent-thick symmetrical circular-arc airfoils with 30-percent-chord trailing-edge flap and includes data obtained from references 1, 2, and 3 and the present tests. The variations of $c_{h\alpha}$ and $c_{h\delta}$ with Mach number were previously reported in reference 11 and are repeated here for the sake of completeness. It may be seen that the results of shock-expansion theory adequately predict these experimental data for either airfoil thickness throughout the Mach number and Reynolds number range of these tests in spite of the known discrepancies between the theoretical and experimental pressure distributions caused by laminar separation.

The Busemann second-order theory. - It is of interest to compare the results of shock-expansion theory with the Busemann approximation or second-order theory presented in reference 12. Such a comparison is made in table II at a Mach number of 6.9 for the present configuration. In general, the experimental results are in better agreement with shock-expansion theory than with the Busemann second-order theory particularly in the case of the flap parameters $c_{m\delta}$ and $c_{h\delta}$ for which the Busemann theory gives poor predictions. A similar comparison was made at a Mach number of 4.04 in reference 3 for both 6- and 9-percent-thick airfoils with comparable results although only in the case of the 9-percent-thick airfoil could the predictions of $c_{m\delta}$ and $c_{h\delta}$ by the Busemann theory be considered poor.

CONCLUSIONS

An investigation, including pressure distributions and schlieren flow photographs, has been made of the flow characteristics over a 6-percent-thick symmetrical circular-arc airfoil section with a 30-percent-chord trailing-edge flap at a Mach number of 6.90 and a Reynolds number of 1.65×10^6 . An analysis of the results indicated the following conclusions:

1. The experimental pressure distributions and schlieren photographs show regions of laminar separation on the low-pressure side of the flap and in the vicinity of the hinge line on that side of the airfoil which is adjacent to the high-pressure side of the flap. At high angles of attack separation occurs on the upper surface of the entire flap and the rear portion of the wing for both positive and negative flap deflections.

2. The experimental pressure distributions are in good agreement with the results of two-dimensional shock-expansion theory except in the regions of flow separation resulting from shock-boundary-layer interaction where agreement is poor.

3. Even though differences occur between the theoretical and the experimental pressure distributions, the results of shock-expansion theory adequately predict the integrated experimental aerodynamic characteristics except in some cases for large flap deflections.

4. In these tests, the trailing-edge flap was continuously effective throughout the test angle range.

Langley Aeronautical Laboratory,
National Advisory Committee for Aeronautics,
Langley Field, Va., February 14, 1956.

REFERENCES

1. Czarnecki, K. R., and Mueller, James N.: Investigation at Mach Number 1.62 of the Pressure Distribution Over a Rectangular Wing With Symmetrical Circular-Arc Section and 30-Percent-Chord Trailing-Edge Flap. NACA RM L9J05, 1950.
2. Czarnecki, K. R., and Mueller, James N.: Investigation at Supersonic Speeds of Some of the Factors Affecting the Flow Over a Rectangular Wing With Symmetrical Circular-Arc Section and 30-Percent-Chord Trailing-Edge Flap. NACA RM L50J18, 1951.
3. Ulmann, Edward F., and Lord, Douglas R.: An Investigation of Flow Characteristics at Mach Number 4.04 Over 6- and 9-Percent-Thick Symmetrical Circular-Arc Airfoils Having 30-Percent-Chord Trailing-Edge Flaps. NACA RM L51D30, 1951.
4. McLellan, Charles H., Williams, Thomas W., and Beckwith, Ivan E.: Investigation of the Flow Through a Single-Stage Two-Dimensional Nozzle in the Langley 11-Inch Hypersonic Tunnel. NACA TN 2223, 1950.
5. McLellan, Charles H., and Williams, Thomas W.: Liquefaction of Air In The Langley 11-Inch Hypersonic Tunnel. NACA TN 3302, 1954.
6. McLellan, Charles H., Williams, Thomas W., and Bertram, Mitchel H.: Investigation of a Two-Step Nozzle in the Langley 11-Inch Hypersonic Tunnel. NACA TN 2171, 1950.
7. Mayer, John P.: A Limit Pressure Coefficient and an Estimation of Limit Forces on Airfoils at Supersonic Speeds. NACA RM L8F23, 1948.
8. Eggers, A. J., Jr., Syvertson, Clarence A., and Kraus, Samuel: A Study of Inviscid Flow About Airfoils at High Supersonic Speeds. NACA Rep. 1123, 1953. (Supersedes NACA TN 2646 by Eggers and Syvertson and NACA TN 2729 by Kraus.)
9. Bertram, Mitchel H.: An Approximate Method for Determining the Displacement Effects and Viscous Drag of Laminar Boundary Layers in Two-Dimensional Hypersonic Flow. NACA TN 2773, 1952.
10. Rott, Nicholas, and Crabtree, L. F.: Simplified Laminar Boundary-Layer Calculations for Bodies of Revolution and for Yawed Wings. Jour. Aero. Sci., vol. 19, no. 8, Aug., 1952, pp. 553-565.

11. Lord, Douglas R., and Czarnecki, K. R.: Recent Information on Flap and Tip Controls. NACA RM L53I17a, 1953.
12. Morrissette, Robert K., and Oborny, Lester F.: Theoretical Characteristics of Two-Dimensional Supersonic Control Surfaces. NACA TN 2486, 1951. (Supersedes NACA RM L8G12.)

TABLE I

EXPERIMENTAL DATA FOR THE 6-PERCENT-THICK SYMMETRICAL CIRCULAR-ARC
AIRFOIL WITH A 30-PERCENT-CHORD TRAILING-EDGE FLAP
 $[M = 6.90; R = 1.65 \times 10^6]$

α , deg	δ , deg	c_l	c_d	c_l/c_d	c_m	$(\frac{x}{c})_{cp}$	c_n
0	0	0.00	0.0025	0.00	0.00	0.375	0.00
	2	.0026	.0026	.985	-.0009	.850	-.0004
	4	.0048	.0028	1.73	-.0019	.888	-.0088
	8	.0114	.0036	3.17	-.0041	.860	-.0202
	12	.0190	.0051	3.73	-.0066	.842	-.0327
	16	.0282	.0076	3.73	-.0098	.838	-.0486
4	-16	.0292	.0066	4.46	.0118	.105	.0164
	-12	.0372	.0058	6.44	.0095	.247	.0045
	-8	.0411	.0057	7.27	.0084	.296	-.0004
	-4	.0450	.0057	7.86	.0067	.351	-.0079
	-2	.0473	.0059	7.97	.0061	.372	-.0117
	0	.0492	.0064	7.69	.0056	.387	-.0143
	2	.0519	.0066	7.85	.0043	.417	-.0198
	4	.0547	.0073	7.53	.0030	.445	-.0258
	8	.0629	.0091	6.92	.0006	.490	-.0374
	12	.0760	.0129	5.89	-.0041	.550	-.0636
	16	.0908	.0185	4.91	-.0092	.594	-.0884
8	-16	.0839	.0166	5.04	.0190	.277	.0029
	-12	.0874	.0164	5.31	.0177	.300	-.0025
	-8	.0911	.0166	5.50	.0166	.319	-.0073
	-4	.0948	.0168	5.64	.0150	.343	-.0149
	-2	.0984	.0174	5.66	.0140	.360	-.0196
	0	.1006	.0180	5.59	.0132	.371	-.0224
	2	.1067	.0192	5.56	.0114	.400	-.0329
	4	.1098	.0204	5.38	.0096	.415	-.0395
	8	.1231	.0245	5.02	.0048	.460	-.0630
	12	.1438	.0319	4.51	-.0020	.511	-.0964
	16	.1640	.0417	3.93	-.0099	.554	-.136
12	-16	.1403	.0347	4.05	.0251	.325	-.0097
	-12	.1451	.0355	4.09	.0253	.330	-.0113
	-8	.1505	.0357	4.21	.0233	.349	-.0216
	-4	.1551	.0374	4.14	.0217	.363	-.0276
	-2	.1598	.0386	4.14	.0206	.374	-.0336
	0	.1651	.0401	4.12	.0189	.388	-.0431
	2	.1696	.0417	4.07	.0164	.4055	-.0544
	4	.1756	.0441	3.98	.0136	.4243	-.0665
	8	.1952	.0521	3.75	.0077	.4608	-.0986
	12	.2208	.0648	3.41	-.0024	.5080	-.145
	16	.2496	.0816	3.06	-.0135	.5467	-.202
16	-16	.207	.0652	3.17	.0372	.327	-.0184
	-12	.211	.0660	3.20	.0354	.339	-.0251
	-8	.217	.0674	3.22	.0334	.353	-.0322
	-4	.226	.0700	3.23	.0296	.375	-.0485
	-2	.232	.0719	3.23	.0276	.386	-.0586
	0	.2379	.0745	3.19	.0249	.401	-.0709
	2	.253	.0797	3.17	.0212	.419	-.0908
	4	.264	.0849	3.11	.0168	.439	-.1128
	8	.289	.0986	2.93	.0077	.474	-.1575
	12	.311	.115	2.70	-.0027	.5056	-.207
	16	.348	.142	2.45	-.0177	.5425	-.278

TABLE II

COMPARISON OF THE EXPERIMENTAL DATA AT ZERO LIFT WITH
 SHOCK-EXPANSION THEORY AND THE BUSEMANN SECOND-ORDER AIRFOIL
 THEORY FOR A 6-PERCENT-THICK SYMMETRICAL CIRCULAR-ARC
 AIRFOIL WITH A 30-PERCENT-CHORD TRAILING-EDGE FLAP
 AT A MACH NUMBER OF 6.90

Aerodynamic characteristics	Experimental results	Shock-expansion theory	Busemann second-order theory
$c_{l\alpha} \dots \dots \dots$	0.012	0.012	0.010
$c_{dp} \dots \dots \dots$	0.0027	0.0030	0.0028
$c_{m\alpha} \dots \dots \dots$	0.0016	0.0016	0.0017
$c_{m\delta} \dots \dots \dots$	-0.00046	-0.00053	-0.00028
$c_{h\delta} \dots \dots \dots$	-0.0026	-0.0026	-0.00103
$c_{lf\delta} \dots \dots \dots$	0.0013	0.0011	0.00094
$(\frac{x}{c})_{cp}$ (for $\frac{\delta}{\alpha} = 1$)	0.41	0.41	0.37

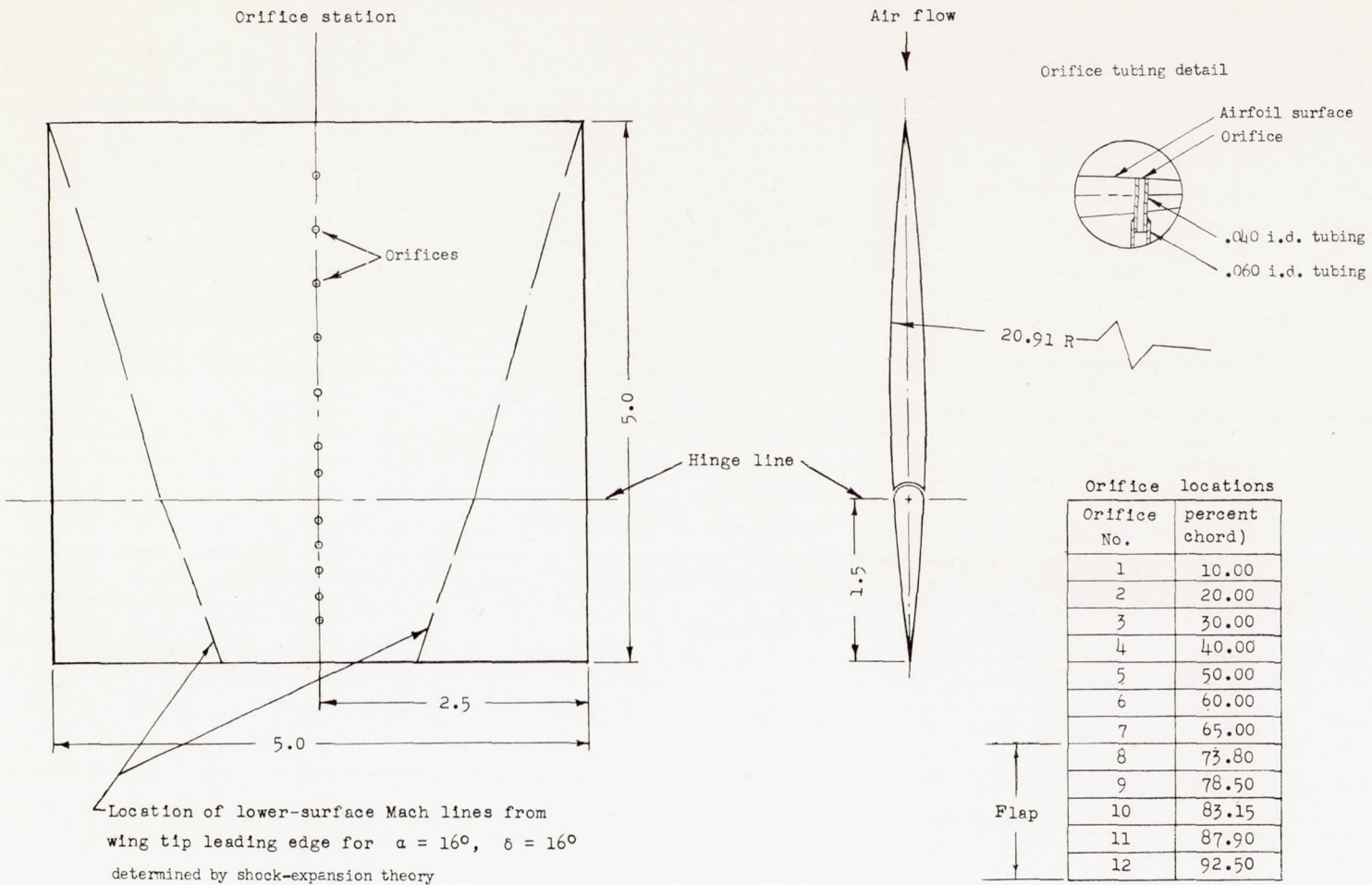


Figure 1.- Dimensions and orifice locations for the 6-percent-thick symmetrical circular-arc airfoil with 30-percent-chord trailing-edge flap used in determining pressure distribution. All dimensions are in inches.

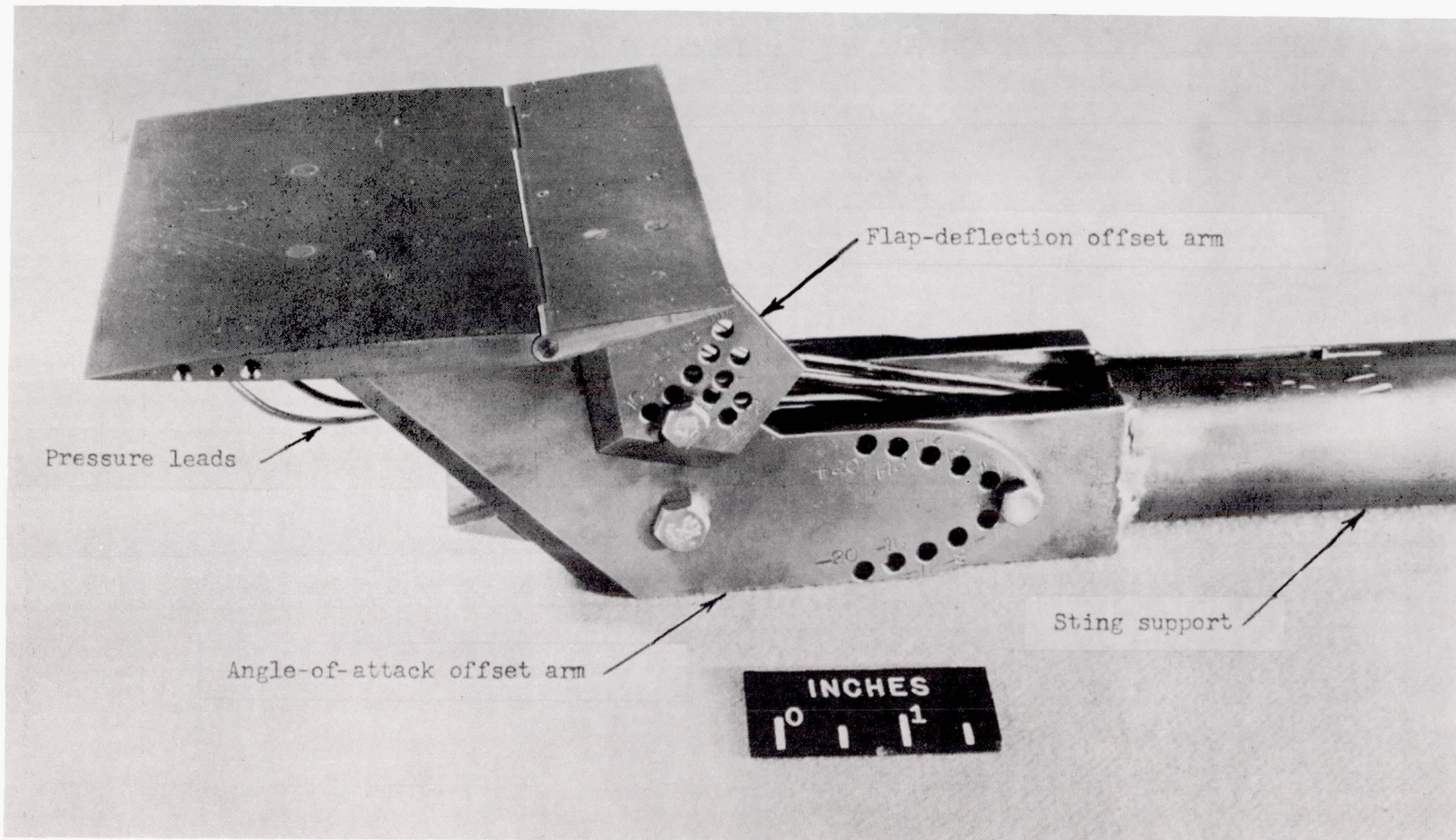


Figure 2.- Photograph of two-dimensional pressure-distribution model and model support system (flap deflected). **L-9026.1**

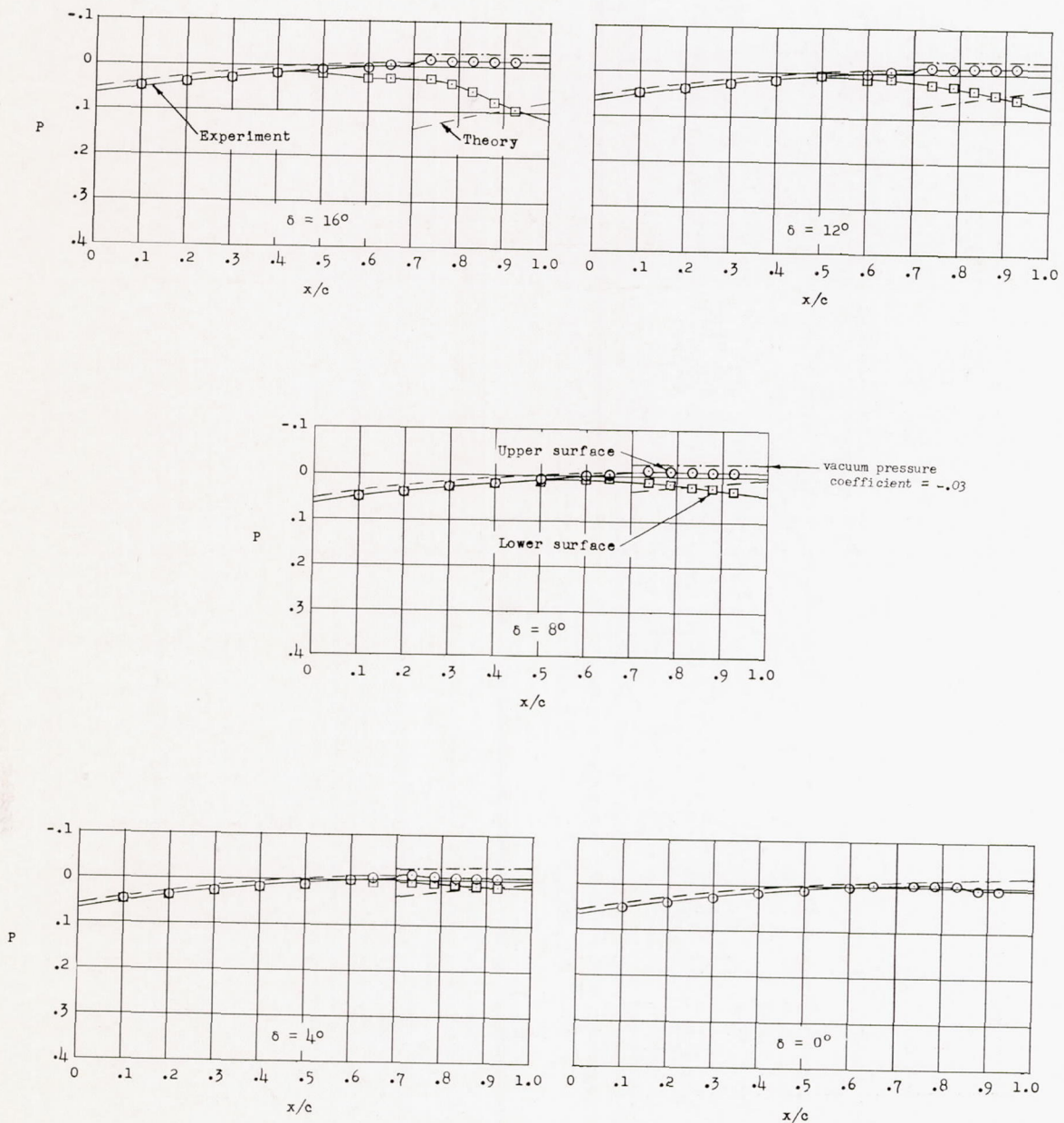
(a) $\alpha = 0^\circ$.

Figure 3.- The effect of flap deflection on the experimental and theoretical pressure distributions over a 6-percent-thick symmetrical circular-arc airfoil with a 30-percent-chord trailing-edge flap.
 $M = 6.90$; $R = 1.65 \times 10^6$.

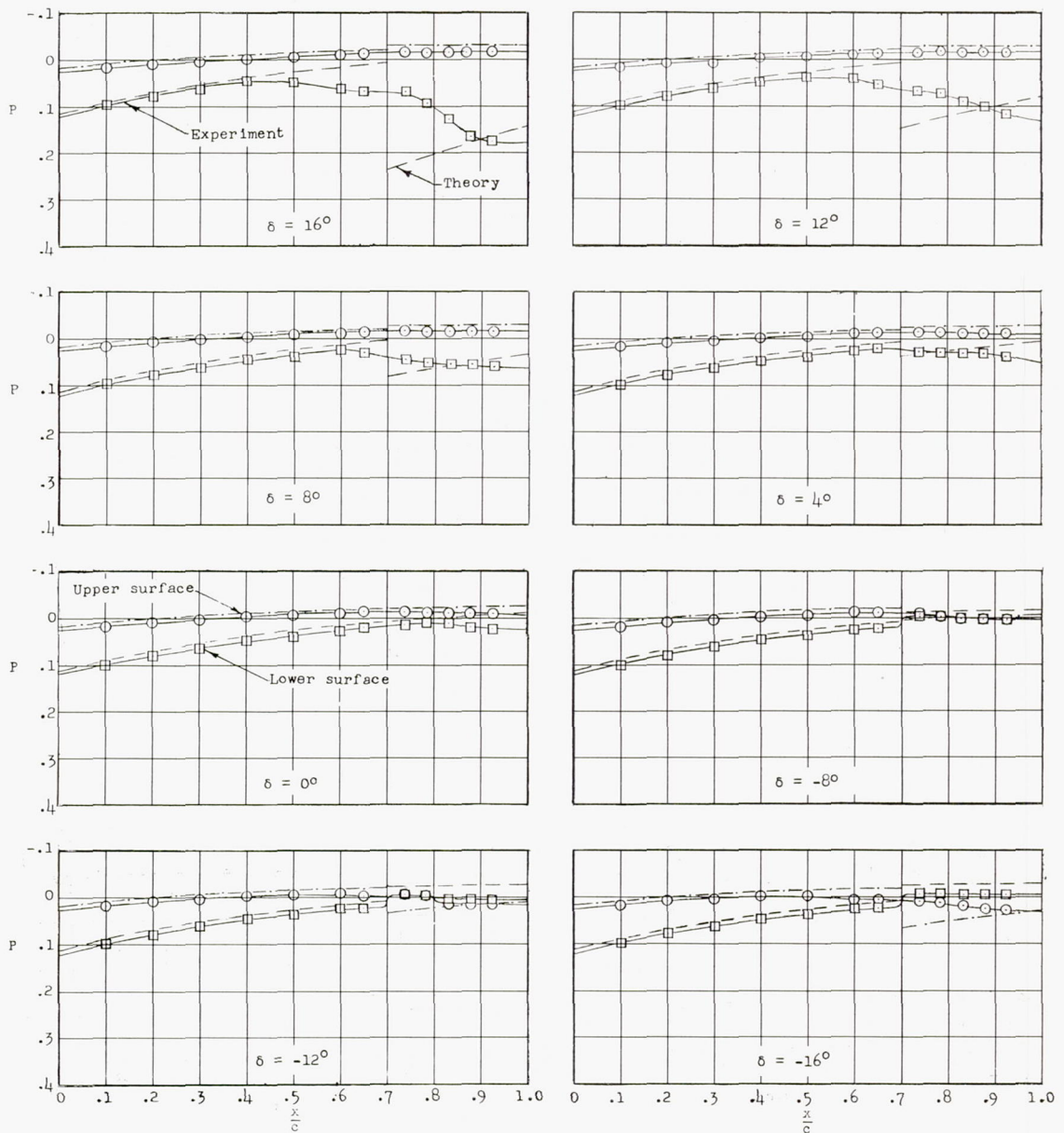
(b) $\alpha = 4^\circ$.

Figure 3.- Continued.

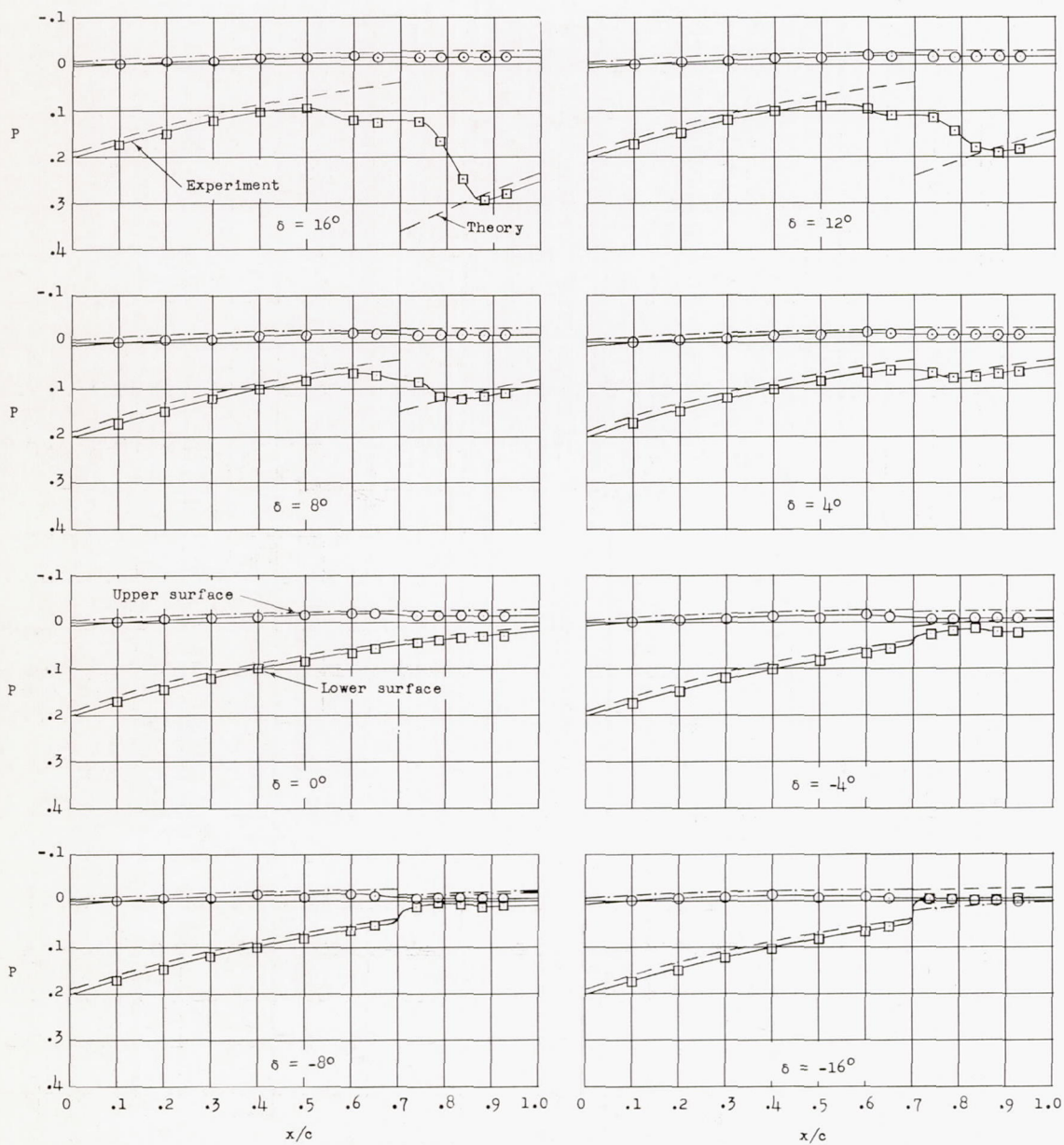
(c) $\alpha = 8^\circ$.

Figure 3.- Continued.

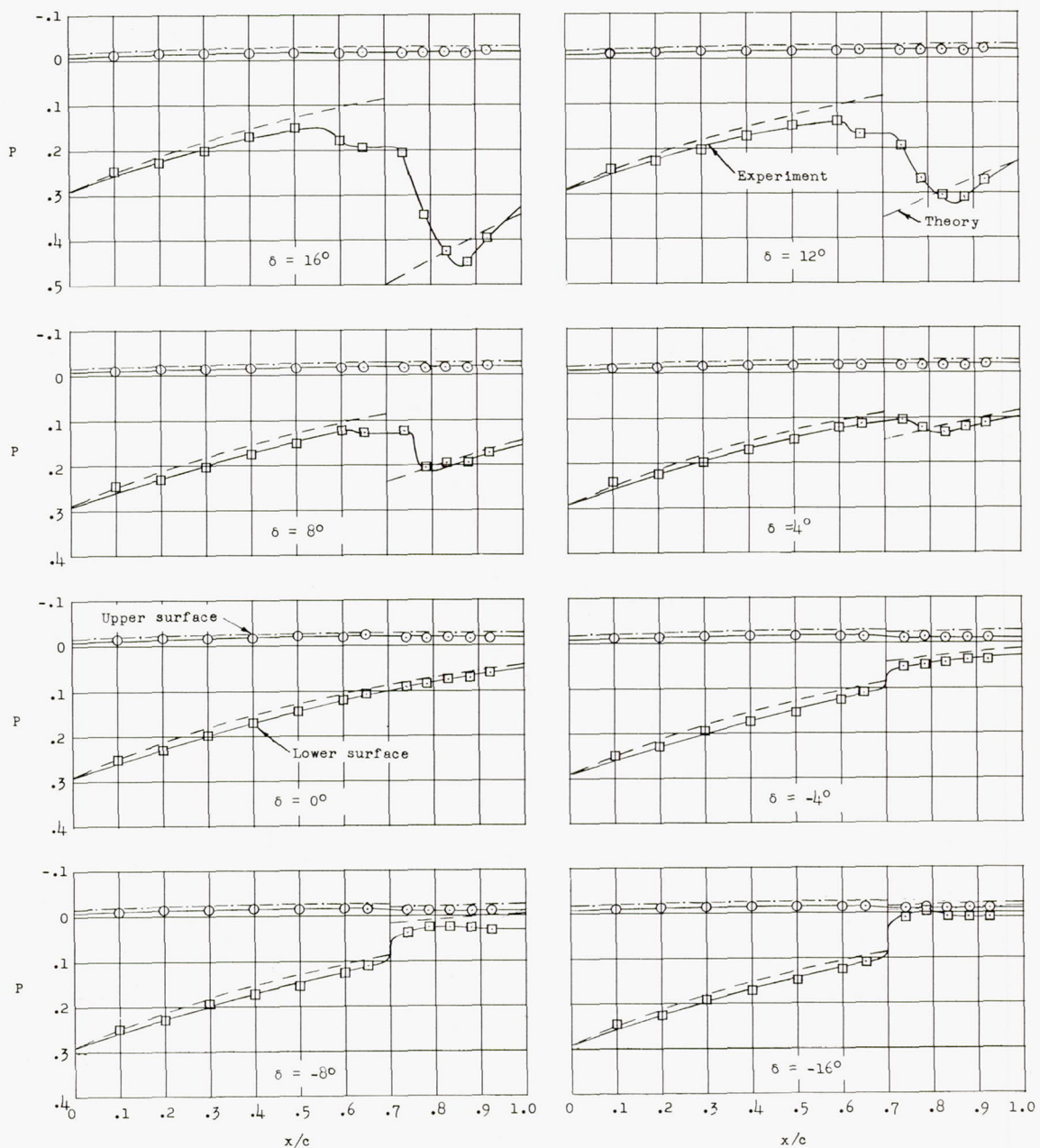
(d) $\alpha = 12^\circ$.

Figure 3.- Continued.

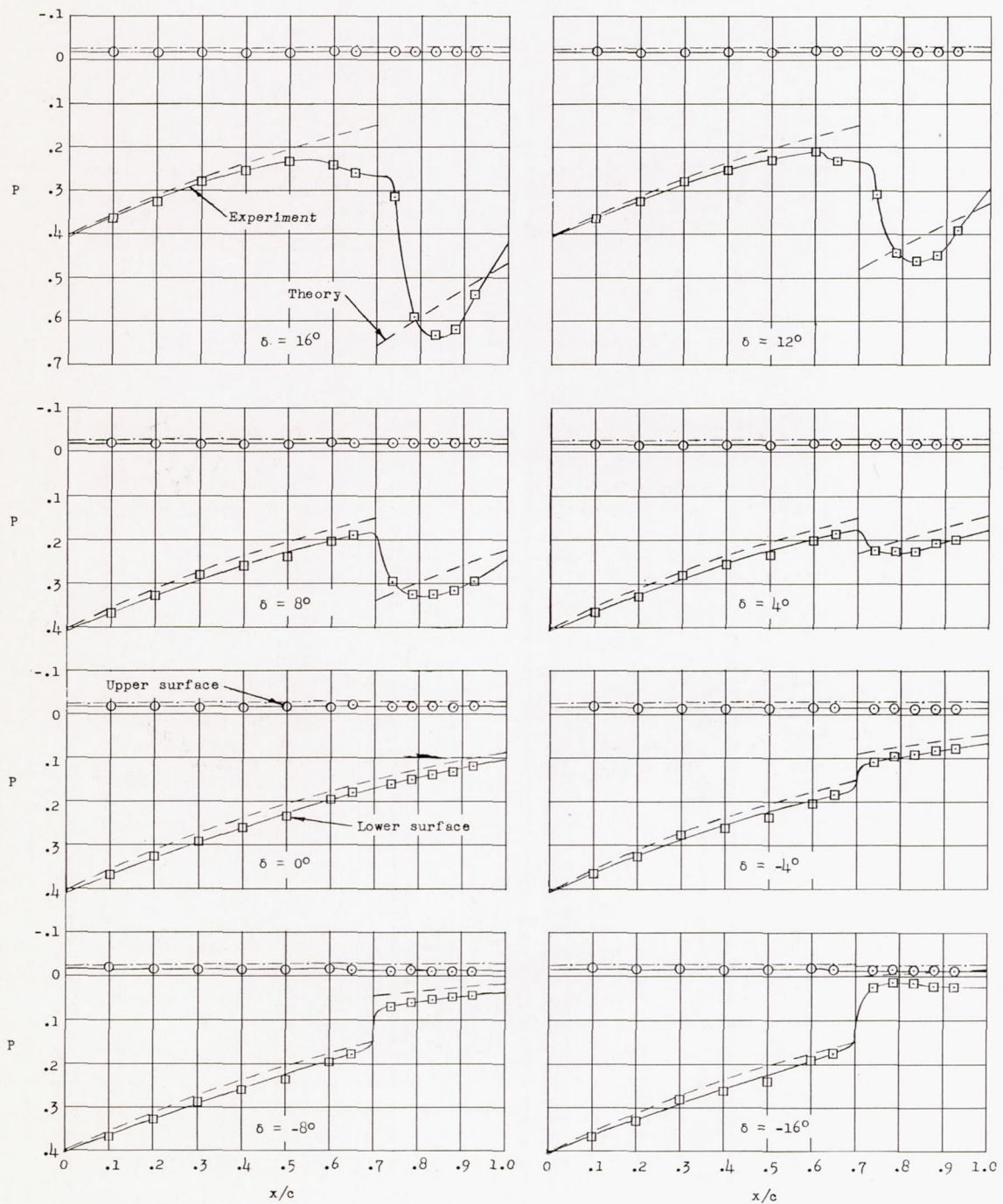
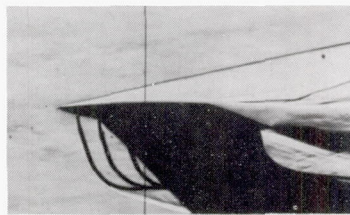
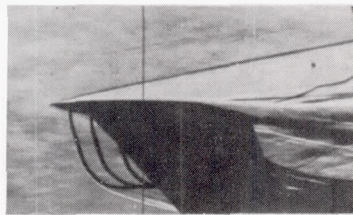
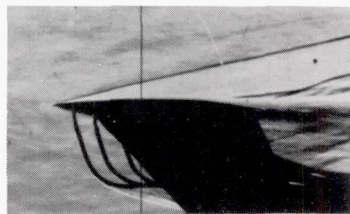
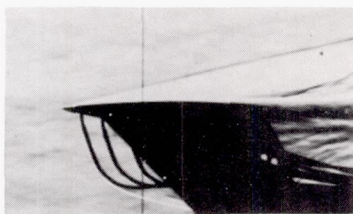
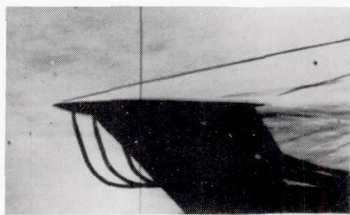
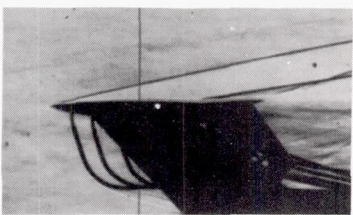
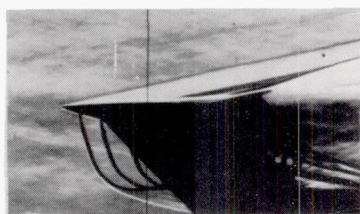
(e) $\alpha = 16^\circ$.

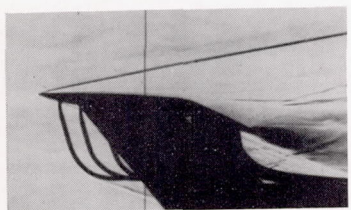
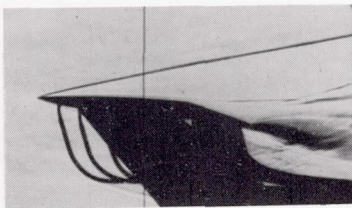
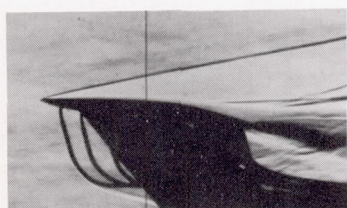
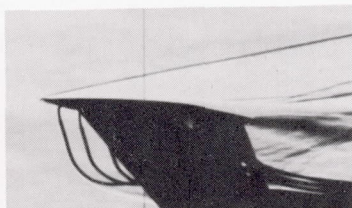
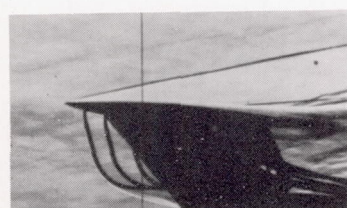
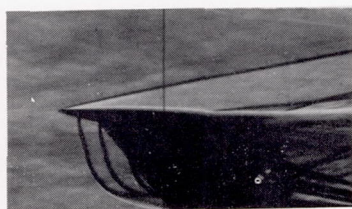
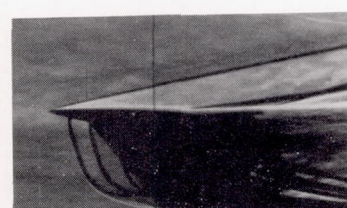
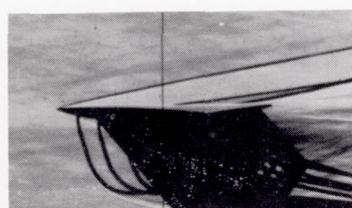
Figure 3.- Concluded.


 $\delta = 16^\circ$

 $\delta = 8^\circ$

 $\delta = 4^\circ$

 $\delta = 0^\circ$

 $\delta = -4^\circ$

 $\delta = -8^\circ$

 $\delta = -16^\circ$

(a) $\alpha = 0^\circ$; upper surface.

L-92417

Figure 4-- Schlieren photographs showing the effect of flap deflection on the flow over the upper surface of an aspect-ratio-1 wing having a 6-percent-thick symmetrical circular-arc airfoil section with a 30-percent-chord trailing-edge flap. $M = 6.90$; $R = 1.65 \times 10^6$.

 $\delta = 16^\circ$  $\delta = 12^\circ$  $\delta = 8^\circ$  $\delta = 4^\circ$  $\delta = 0^\circ$  $\delta = -8^\circ$  $\delta = -12^\circ$  $\delta = -16^\circ$ (b) $\alpha = 4^\circ$; upper surface.

L-92418

Figure 4.- Continued.

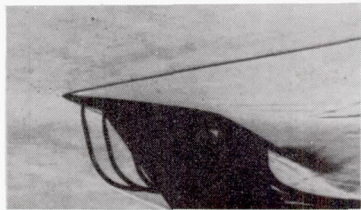
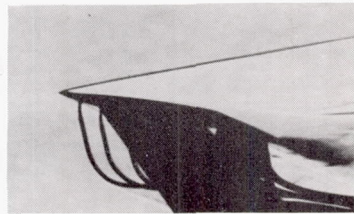
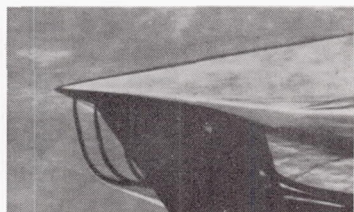
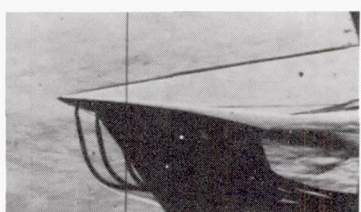
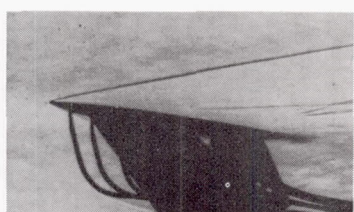
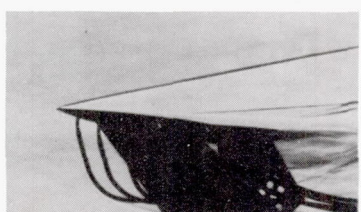
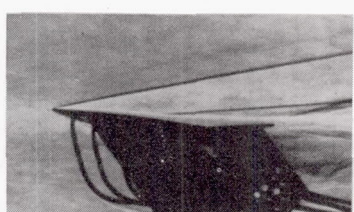
 $\delta = 16^\circ$  $\delta = 12^\circ$  $\delta = 8^\circ$  $\delta = 4^\circ$  $\delta = 0^\circ$  $\delta = -4^\circ$  $\delta = -8^\circ$  $\delta = -16^\circ$ (c) $\alpha = 8^\circ$; upper surface.**L-92419**

Figure 4.- Continued.

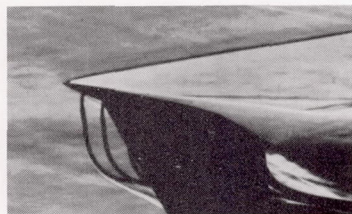
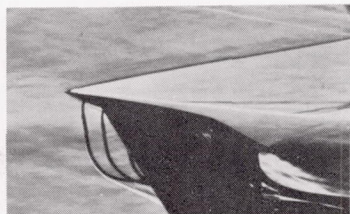
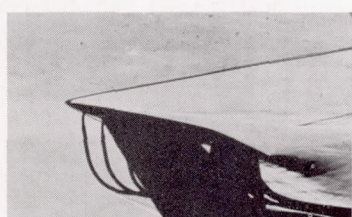
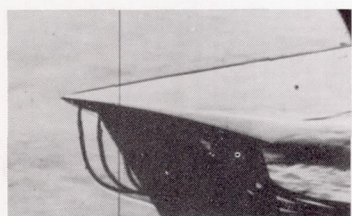
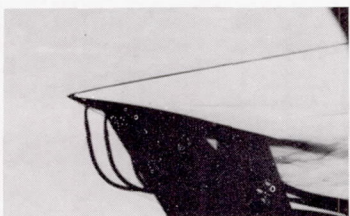
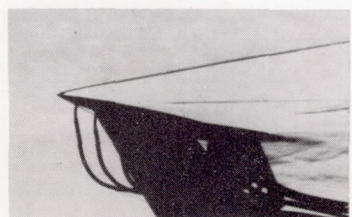
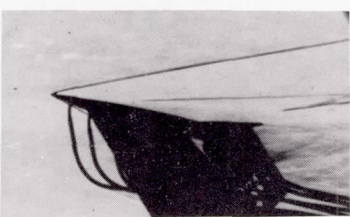
 $\delta = 16^\circ$  $\delta = 12^\circ$  $\delta = 8^\circ$  $\delta = 4^\circ$  $\delta = 0^\circ$  $\delta = -4^\circ$  $\delta = -8^\circ$  $\delta = -16^\circ$ (d) $\alpha = 12^\circ$; upper surface.**L-92420**

Figure 4.- Continued.

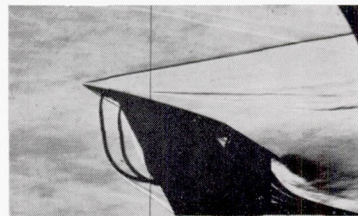
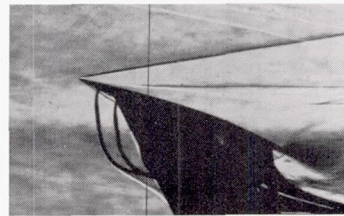
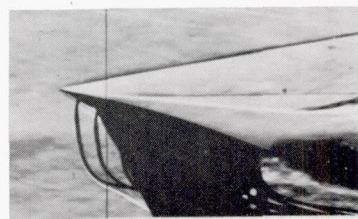
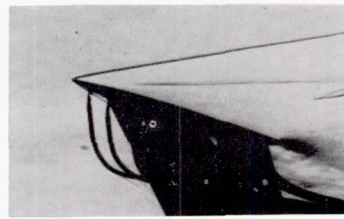
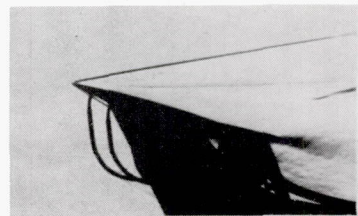
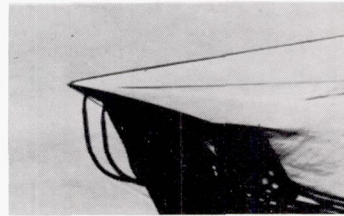
 $\delta = 12^\circ$  $\delta = 4^\circ$  $\delta = 0^\circ$  $\delta = -4^\circ$  $\delta = -12^\circ$  $\delta = -16^\circ$ (e) $\alpha = 16^\circ$; upper surface.**L-92421**

Figure 4.- Concluded.

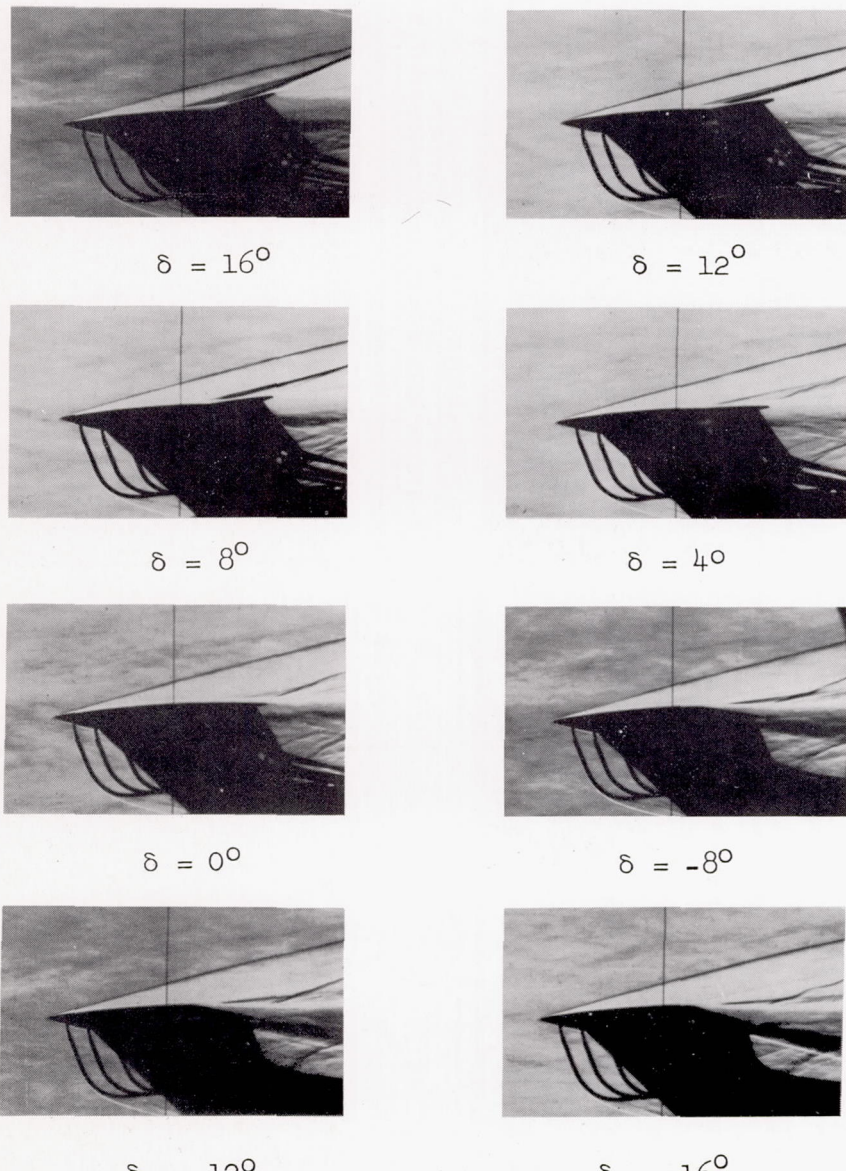
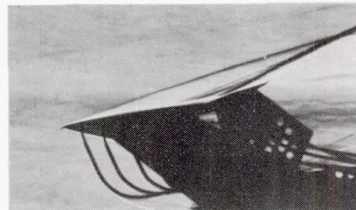
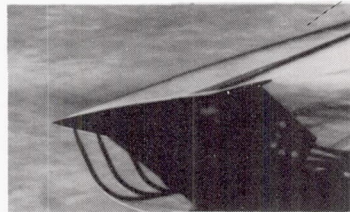
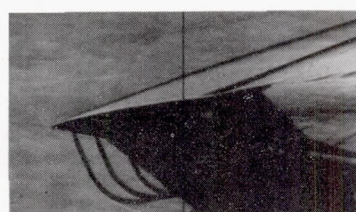
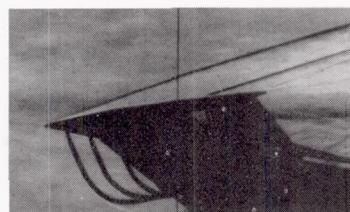
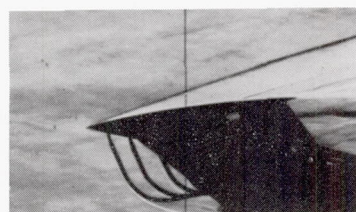
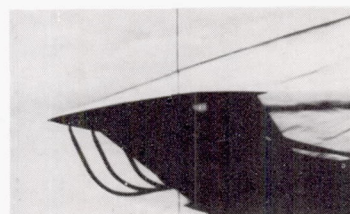
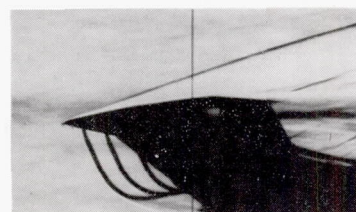
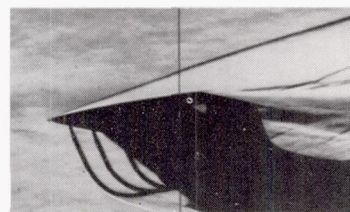
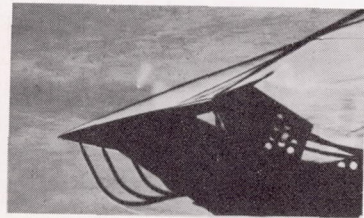
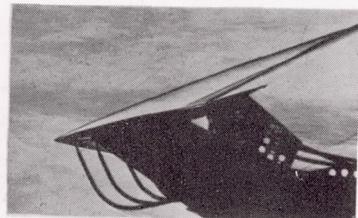
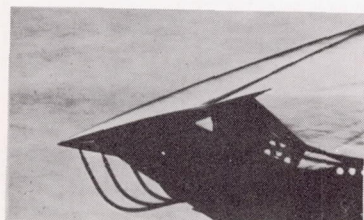
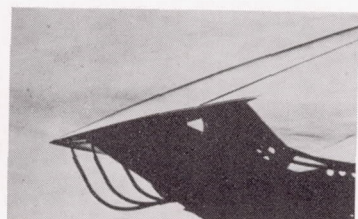
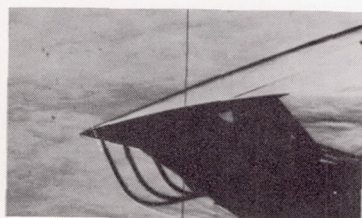
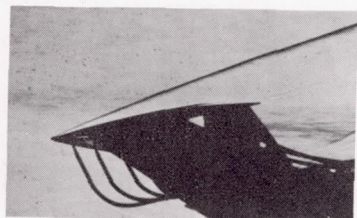
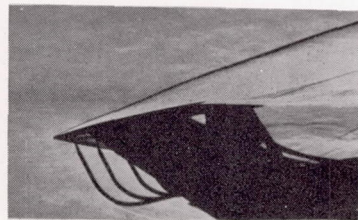
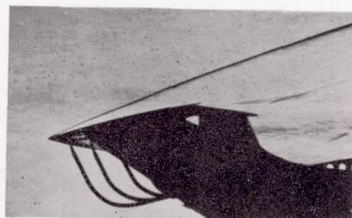
(a) $\alpha = 4^\circ$; lower surface.**L-92422**

Figure 5.- Schlieren photographs showing the effect of flap deflection on the flow over the lower surface of an aspect-ratio-1 wing having a 6-percent-thick symmetrical circular-arc airfoil section with a 30-percent-chord trailing-edge flap. $M = 6.90$; $R = 1.65 \times 10^6$.

 $\delta = 16^\circ$  $\delta = 12^\circ$  $\delta = 8^\circ$  $\delta = 4^\circ$  $\delta = 0^\circ$  $\delta = -4^\circ$  $\delta = -8^\circ$  $\delta = -16^\circ$ (b) $\alpha = 8^\circ$; lower surface.

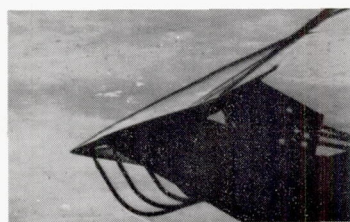
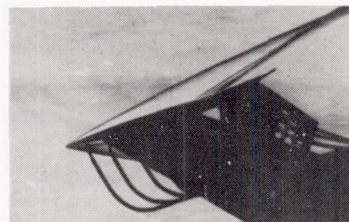
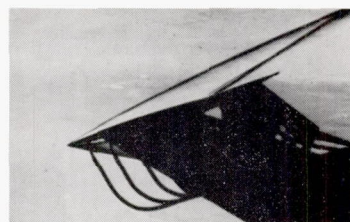
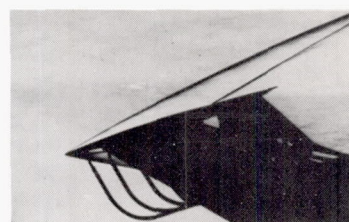
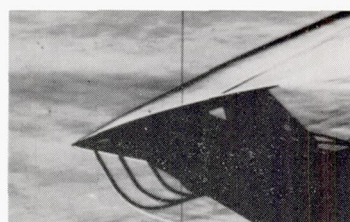
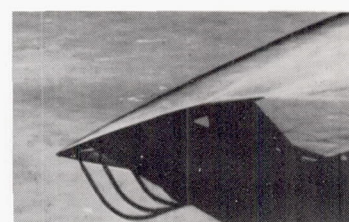
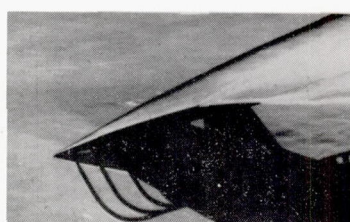
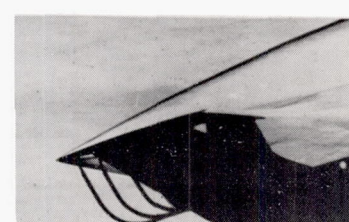
L-92423

Figure 5.- Continued.

 $\delta = 16^\circ$  $\delta = 12^\circ$  $\delta = 8^\circ$  $\delta = 4^\circ$  $\delta = 0^\circ$  $\delta = -4^\circ$  $\delta = -8^\circ$  $\delta = -16^\circ$ (c) $\alpha = 12^\circ$; lower surface.

L-92424

Figure 5.- Continued.

 $\delta = 16^\circ$  $\delta = 12^\circ$  $\delta = 8^\circ$  $\delta = 4^\circ$  $\delta = 0^\circ$  $\delta = -4^\circ$  $\delta = -8^\circ$  $\delta = -16^\circ$ (d) $\alpha = 16^\circ$; lower surface.

L-92425

Figure 5.- Concluded.

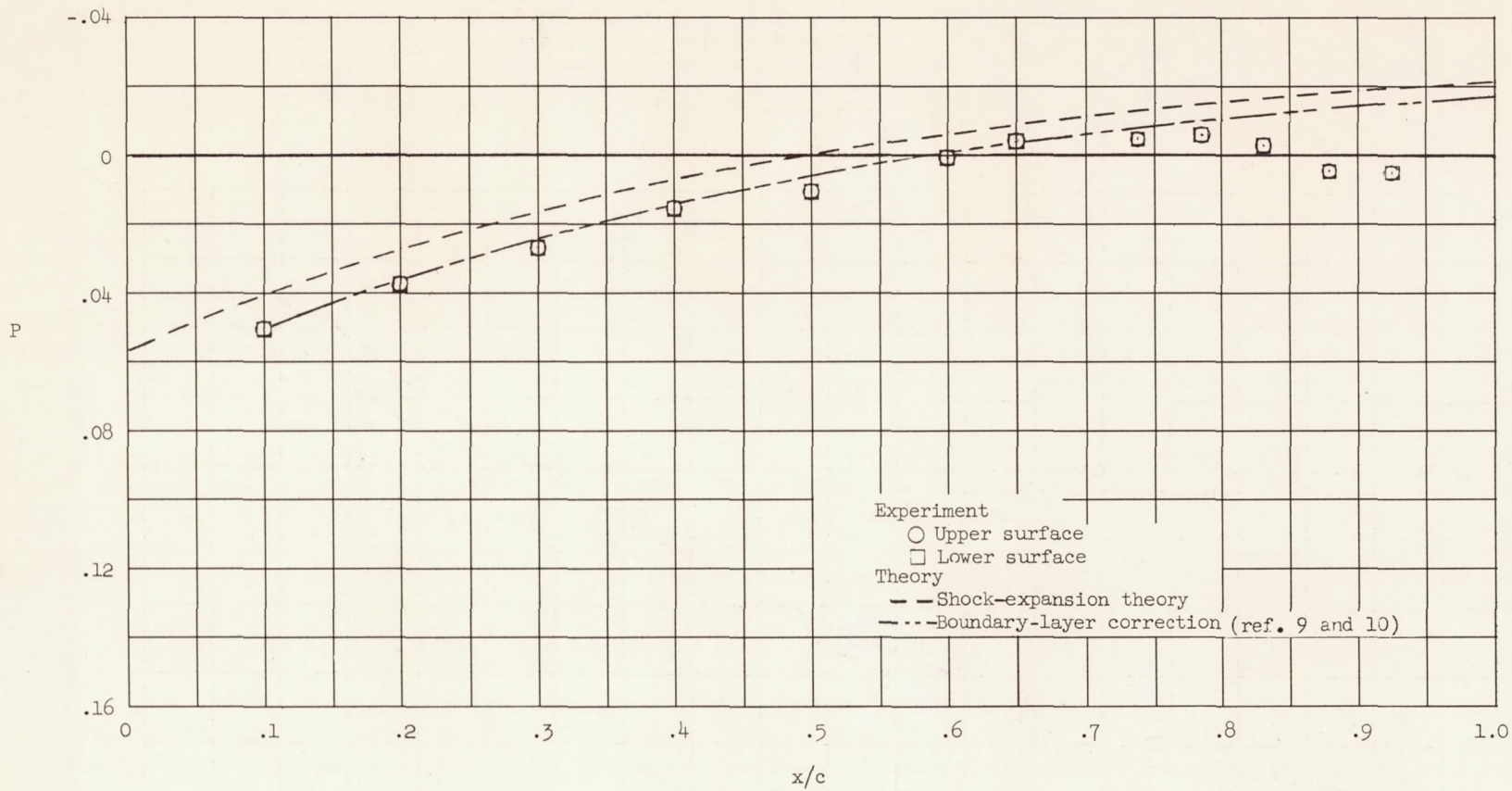
(a) $\alpha = 0^\circ$.

Figure 6.- Experimental and theoretical pressure distributions in a region of two-dimensional flow on a 6-percent-thick symmetrical circular-arc airfoil. $M = 6.90$; $R = 1.65 \times 10^6$; $\delta = 0^\circ$.

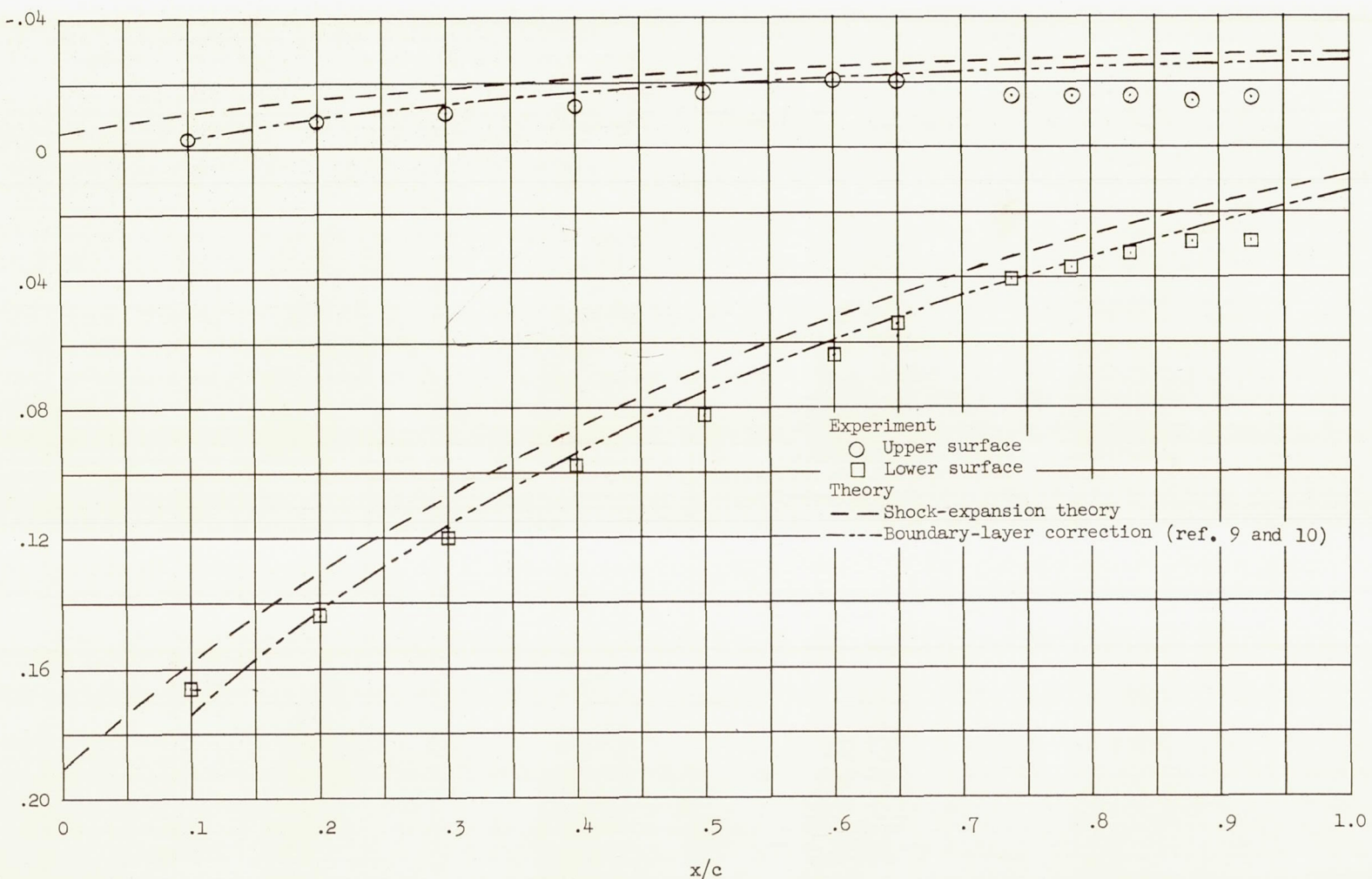
(b) $\alpha = 8^\circ$.

Figure 6.- Concluded.

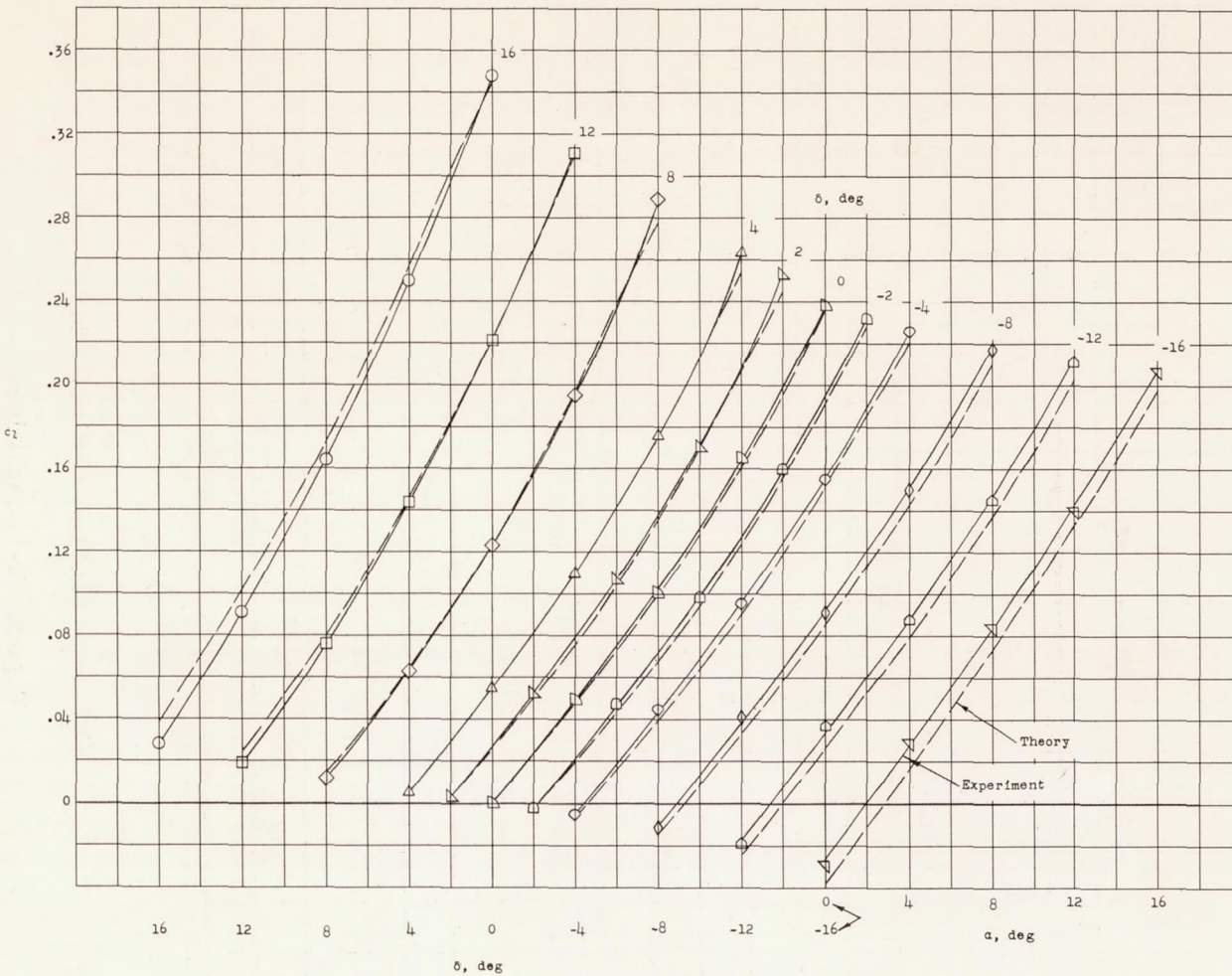
(a) c_l plotted against α .

Figure 7.- The variation of section lift coefficient with angle of attack and flap angle for a 6-percent-thick symmetrical circular-arc airfoil with a 30-percent-chord trailing-edge flap. $M = 6.90$; $R = 1.65 \times 10^6$.

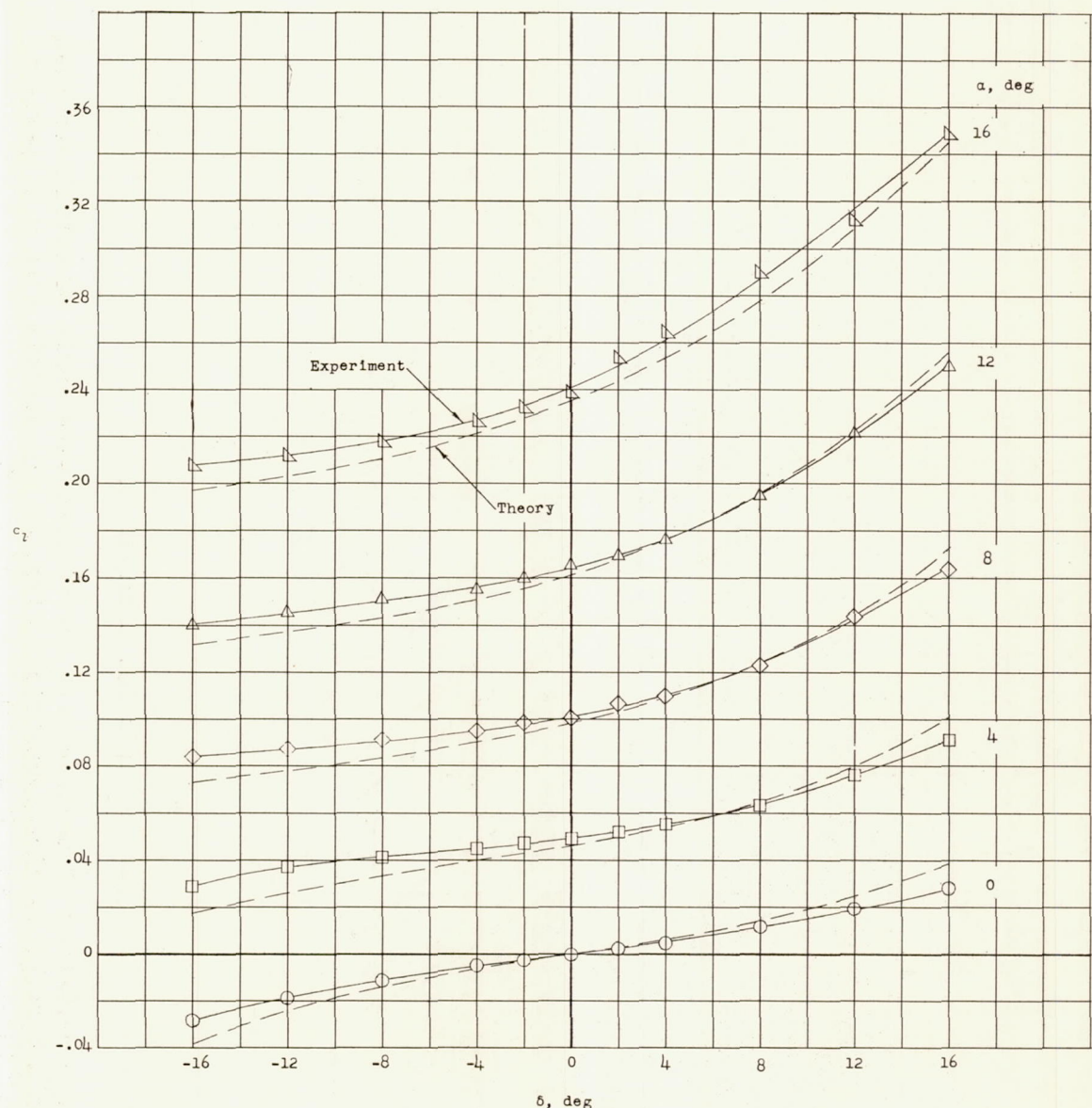
(b) c_l plotted against δ .

Figure 7.- Concluded.

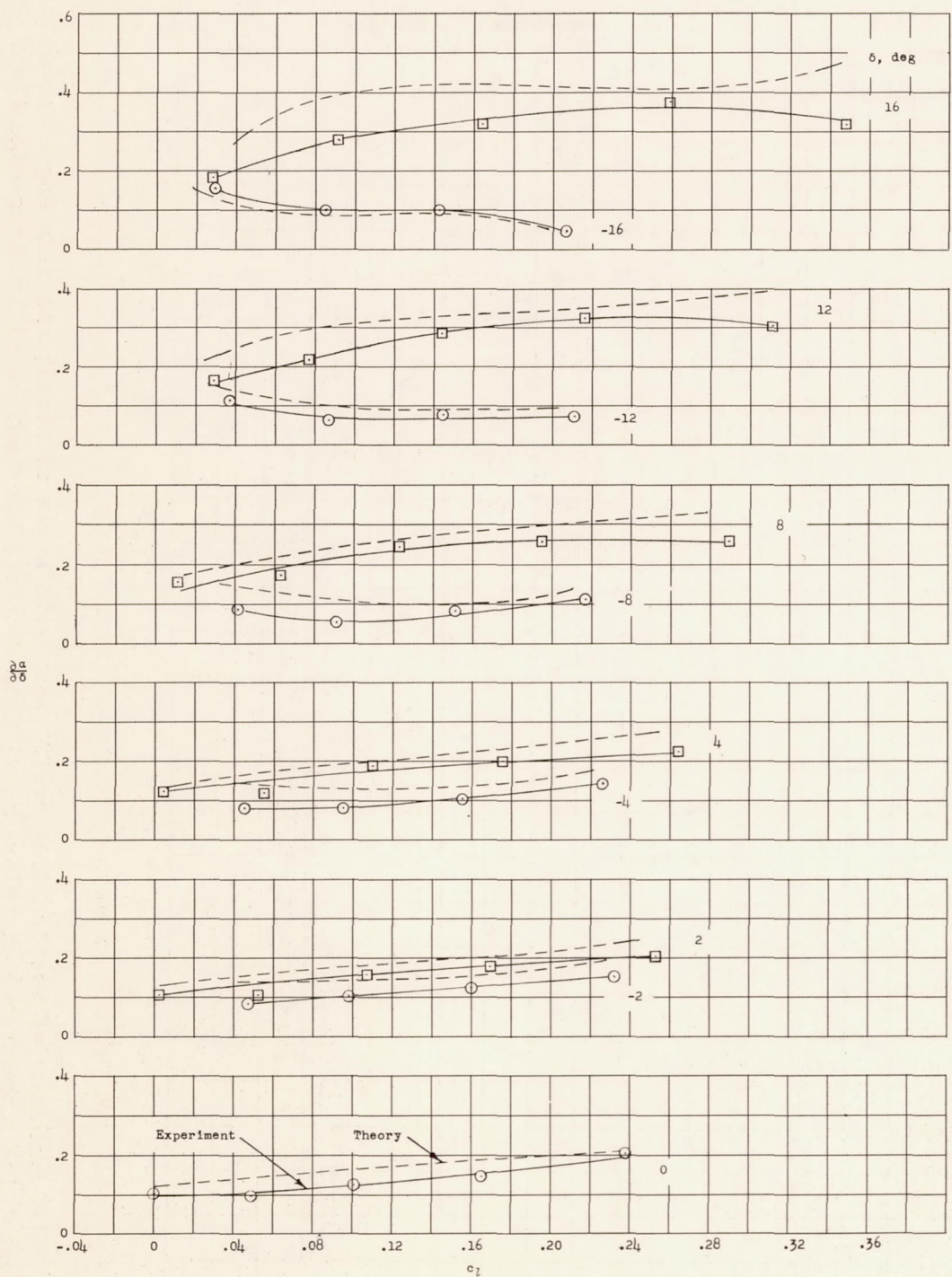


Figure 8.- The variation of the flap effectiveness factor with section lift coefficient at several flap angles for a 6-percent-thick symmetrical circular-arc airfoil with a 30-percent-chord trailing-edge flap.
 $M = 6.90$; $R = 1.65 \times 10^6$.

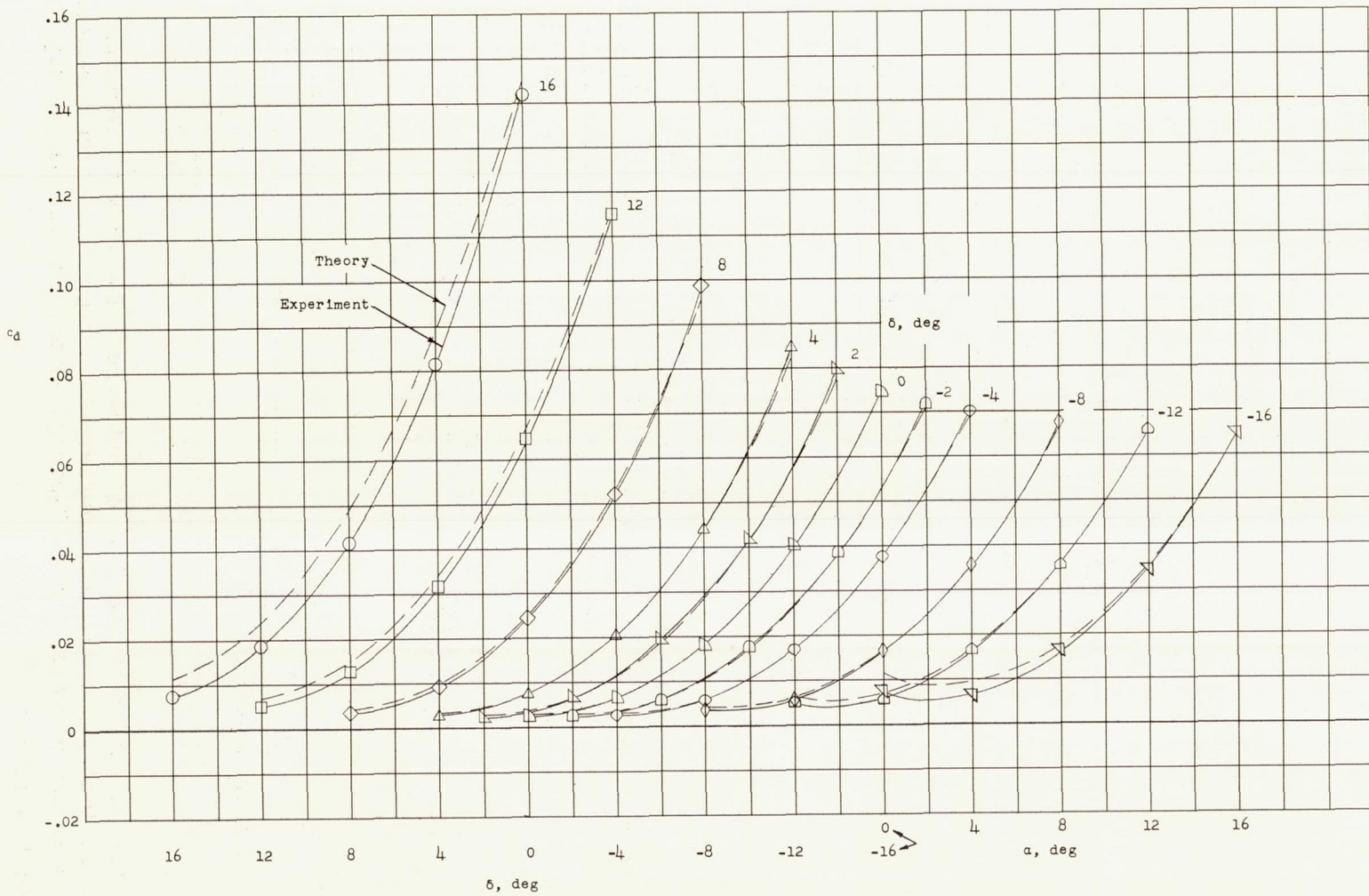


Figure 9.- The variation of section drag coefficient with angle of attack and flap angle for a 6-percent-thick symmetrical circular-arc airfoil with a 30-percent-chord trailing-edge flap.
 $M = 6.90$; $R = 1.65 \times 10^6$.

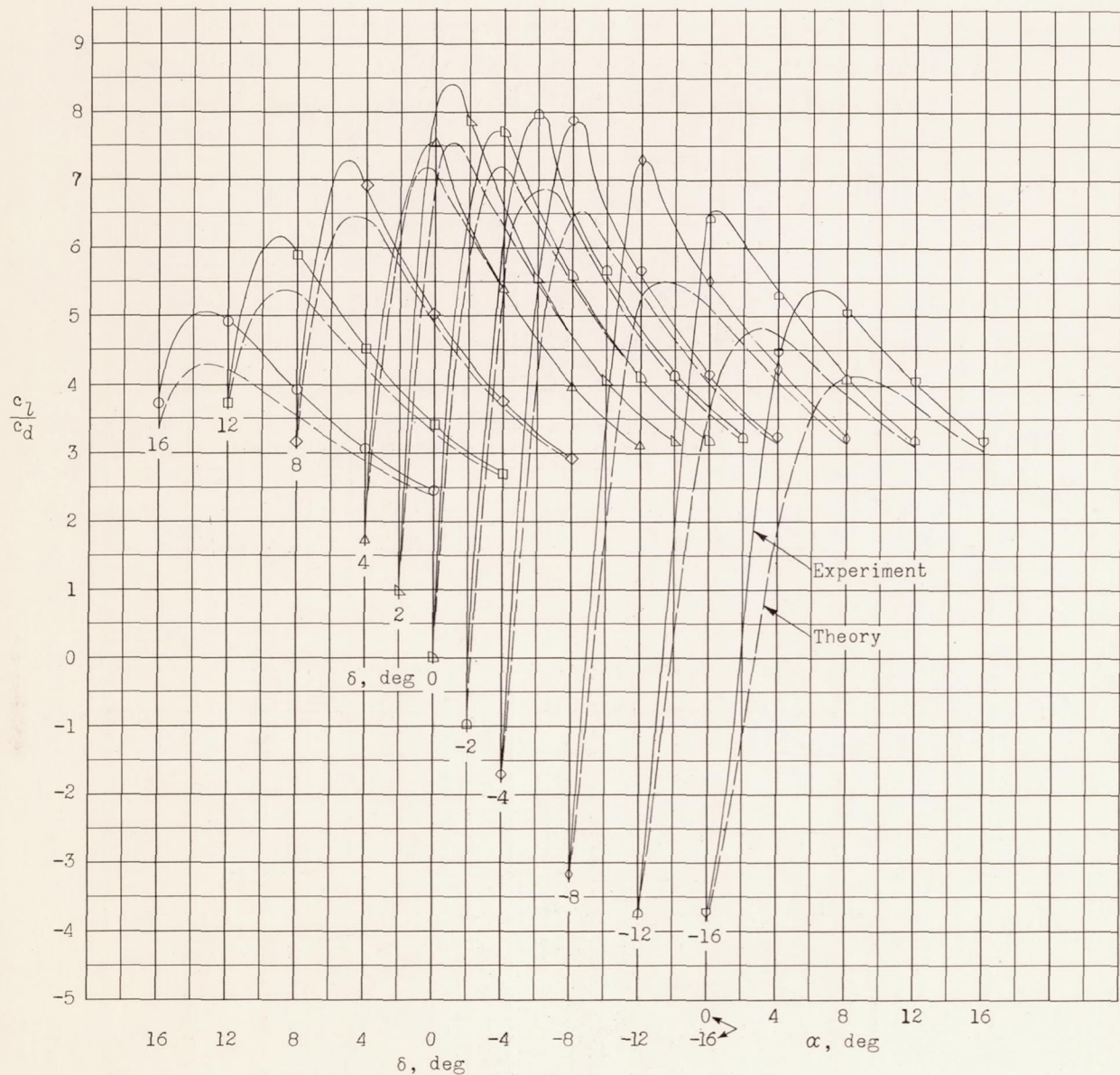


Figure 10.- The variation of section lift-drag ratio with angle of attack and flap angle for a 6-percent-thick symmetrical circular-arc airfoil with a 30-percent-chord trailing-edge flap. $M = 6.90$; $R = 1.65 \times 10^6$.

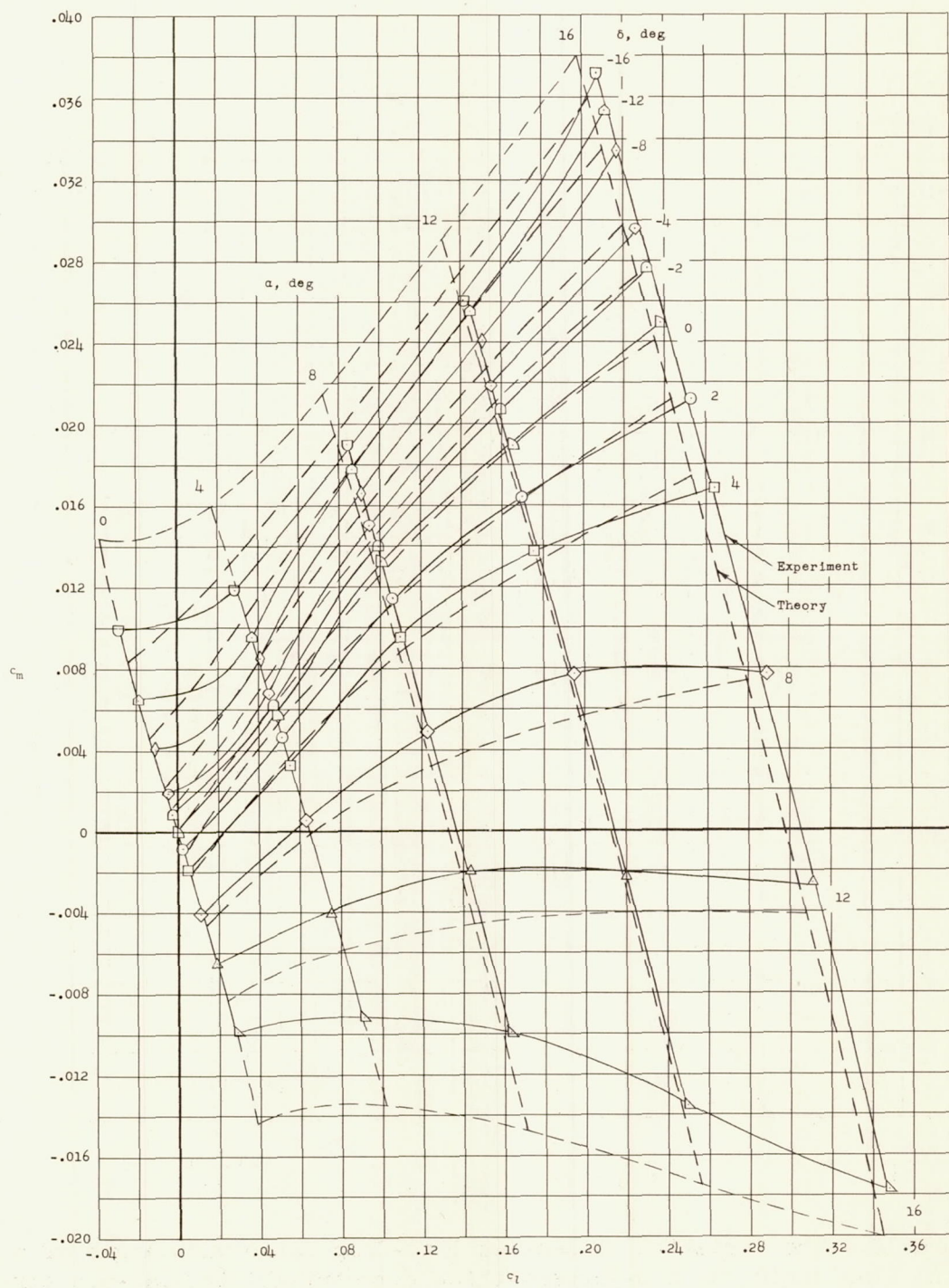


Figure 11.- The variation of section pitching moment with section lift coefficient for constant angles of attack and flap angles for a 6-percent-thick symmetrical circular-arc airfoil with a 30-percent-chord trailing-edge flap. $M = 6.90$; $R = 1.65 \times 10^6$.

CONFIDENTIAL

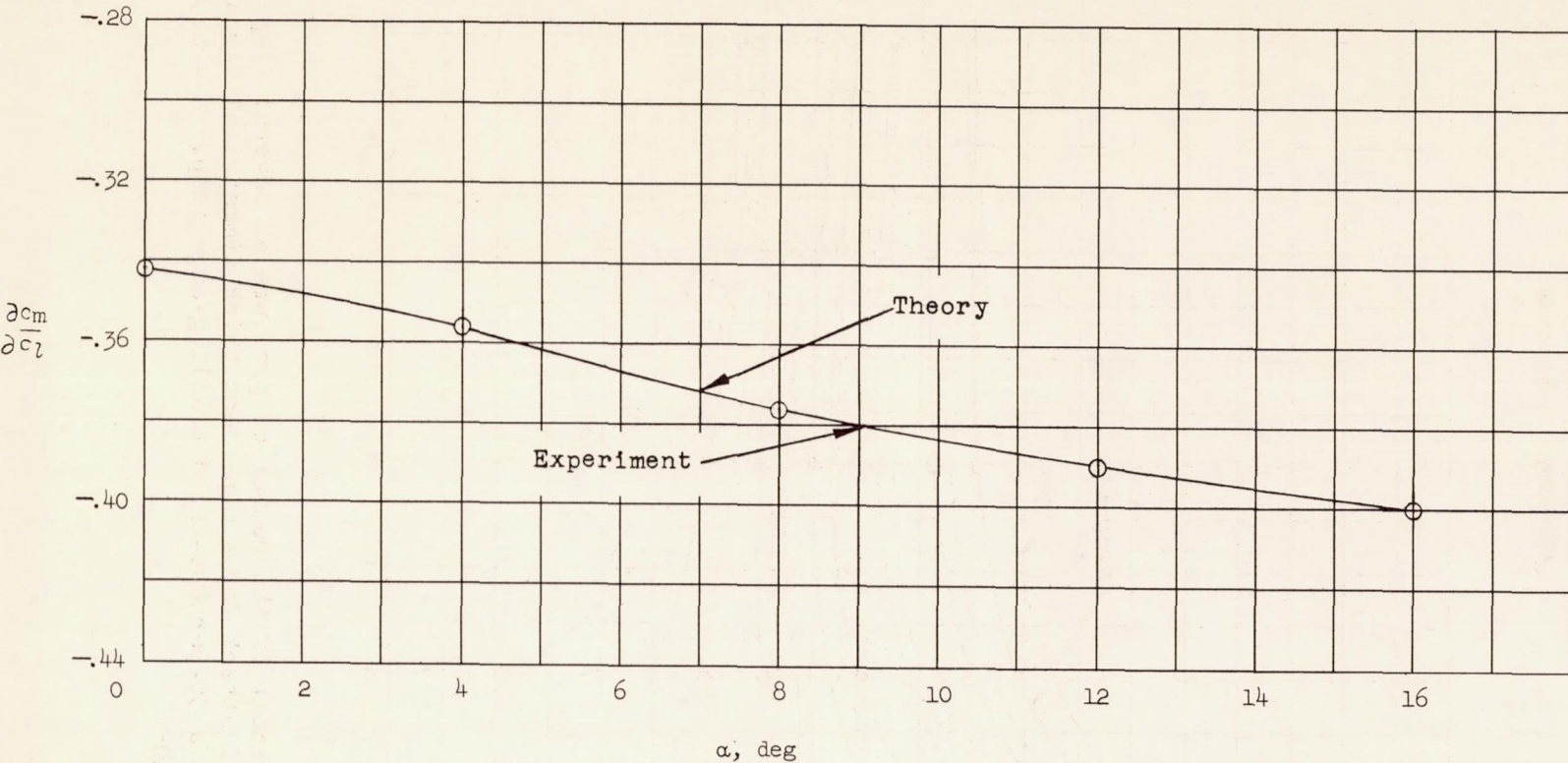


Figure 12.- The rate of change of section pitching moment with section lift coefficient at zero pitching moment and constant angle of attack for a 6-percent-thick symmetrical circular-arc airfoil with a 30-percent-chord trailing-edge flap. $M = 6.90$; $R = 1.65 \times 10^6$.

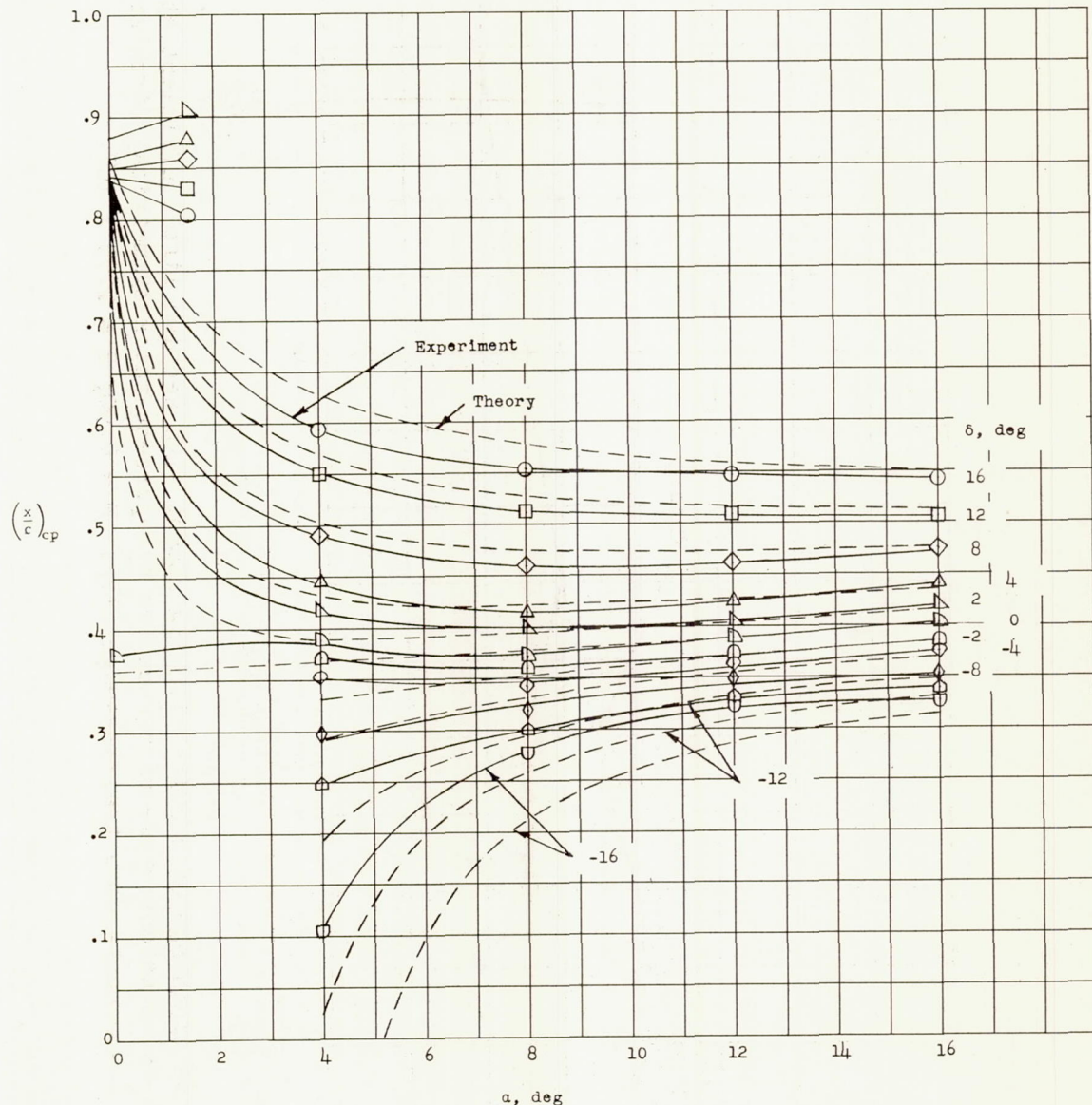


Figure 13.- Movement of the center of pressure at several flap angles with angle of attack for a 6-percent-thick symmetrical circular-arc airfoil with a 30-percent-chord trailing-edge flap. $M = 6.90$; $R = 1.65 \times 10^6$.

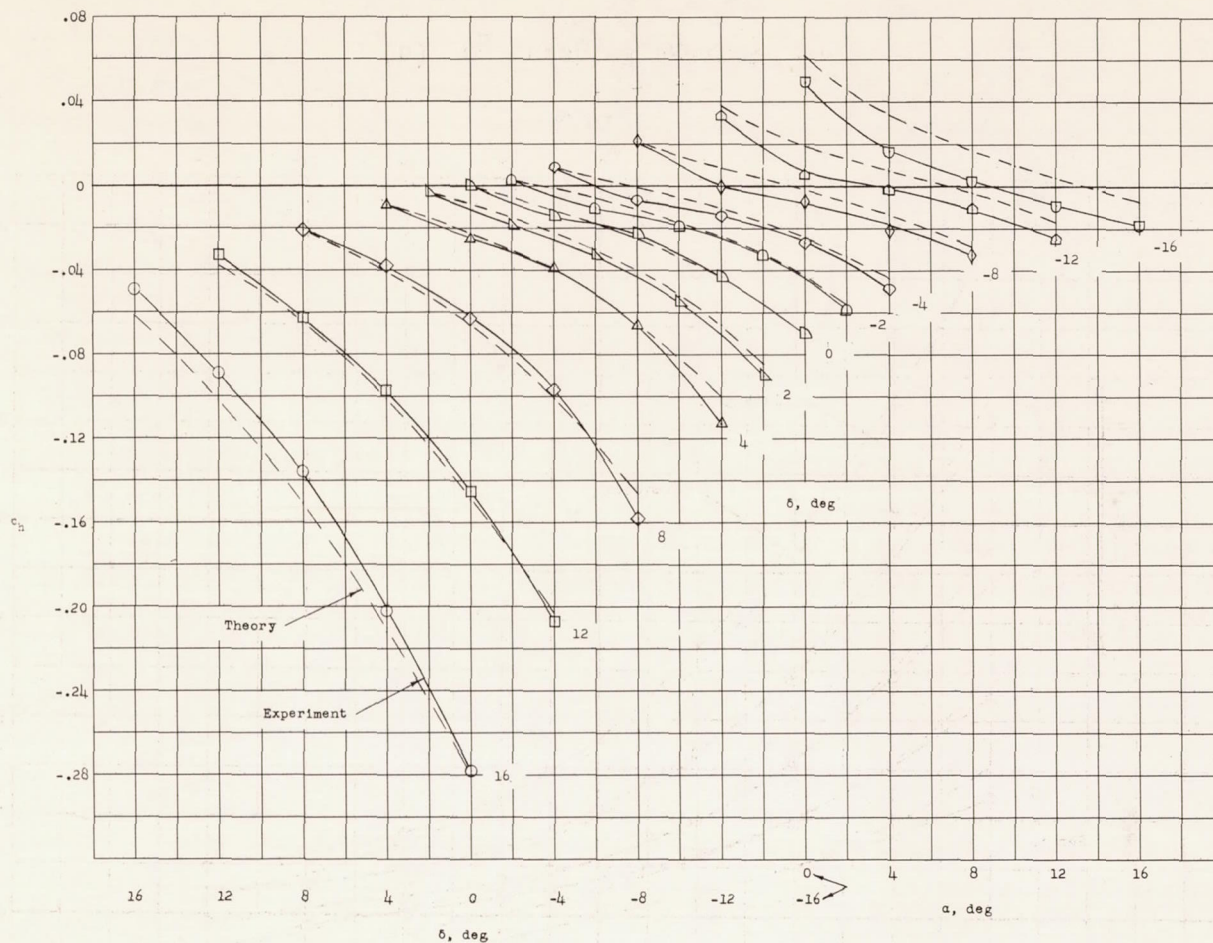
(a) c_h plotted against α .

Figure 14.- The variation of section hinge-moment coefficient with angle of attack and flap angle for a 6-percent-thick symmetrical circular-arc airfoil with a 30-percent-chord trailing-edge flap. $M = 6.90$; $R = 1.65 \times 10^6$.

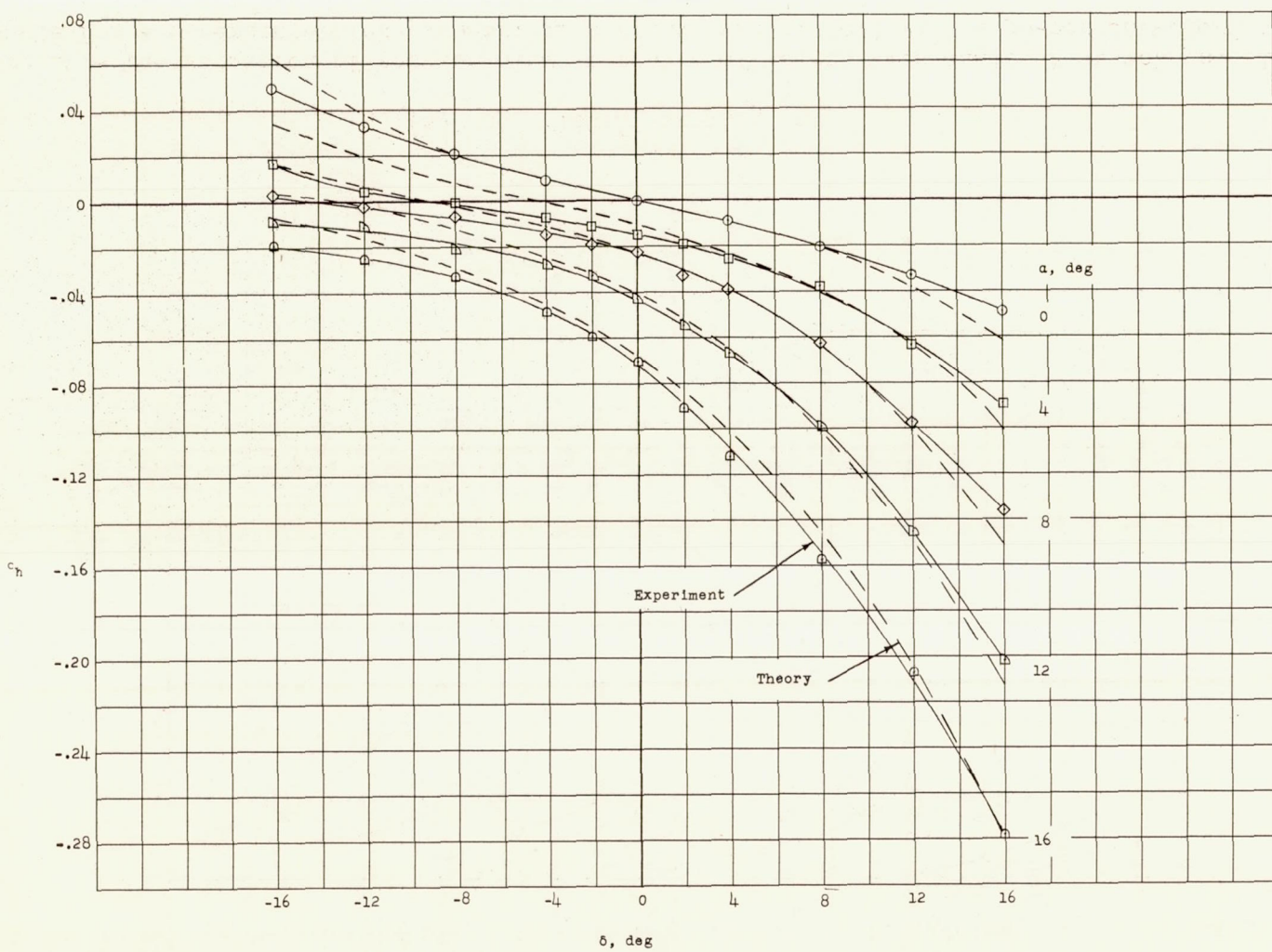
(b) c_h plotted against δ .

Figure 14.- Concluded.

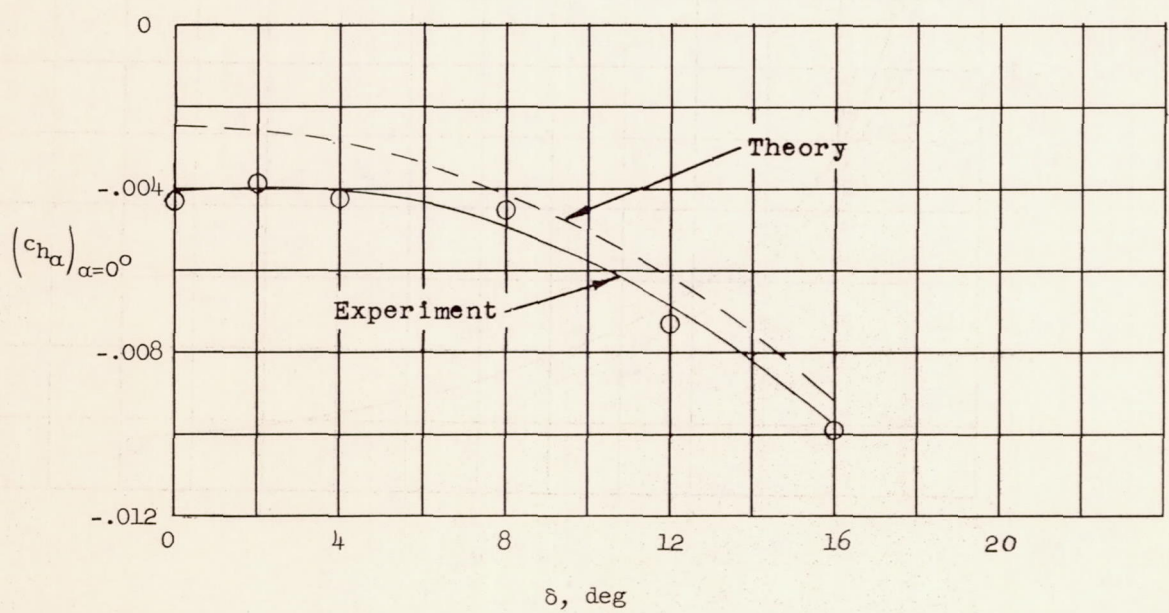
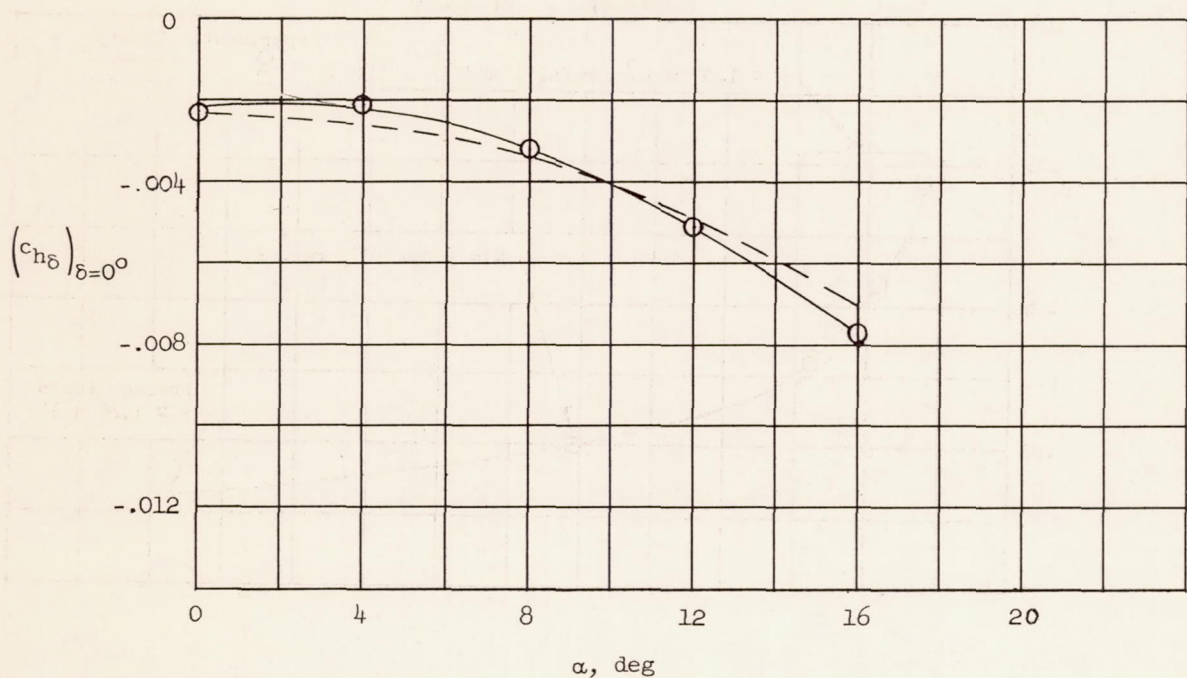


Figure 15.- The variations of section hinge-moment slope parameters $c_{h\delta}$ and $c_{h\alpha}$ with angle of attack and flap deflection, respectively, for a 6-percent-thick symmetrical circular-arc airfoil with a 30-percent-chord trailing-edge flap. $M = 6.90$; $R = 1.65 \times 10^6$.

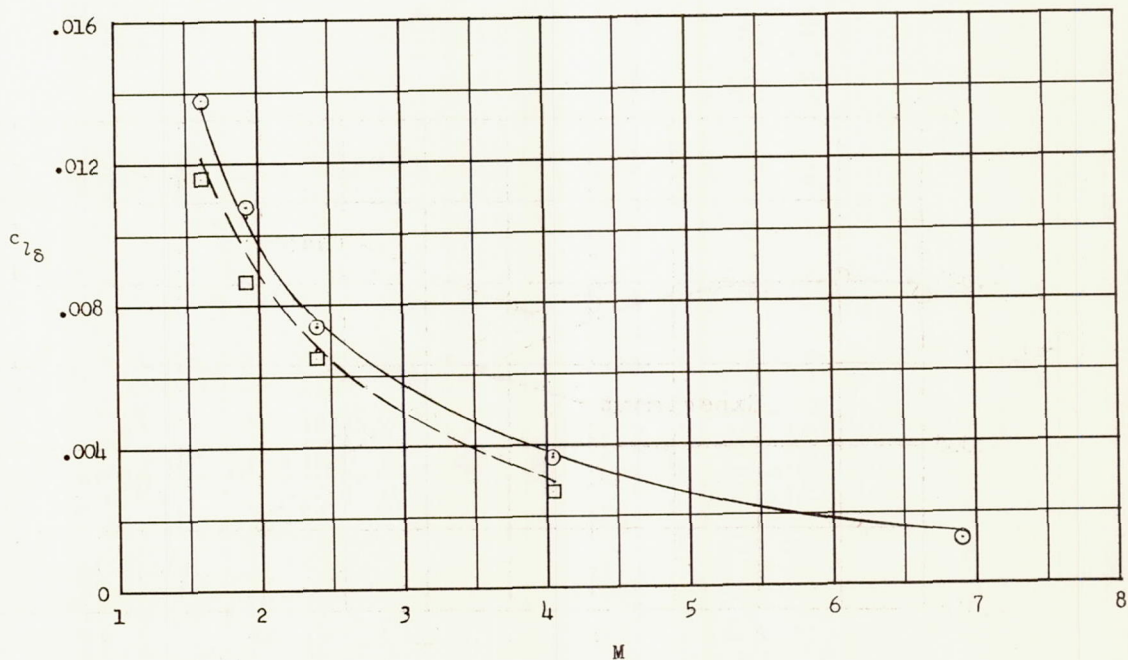
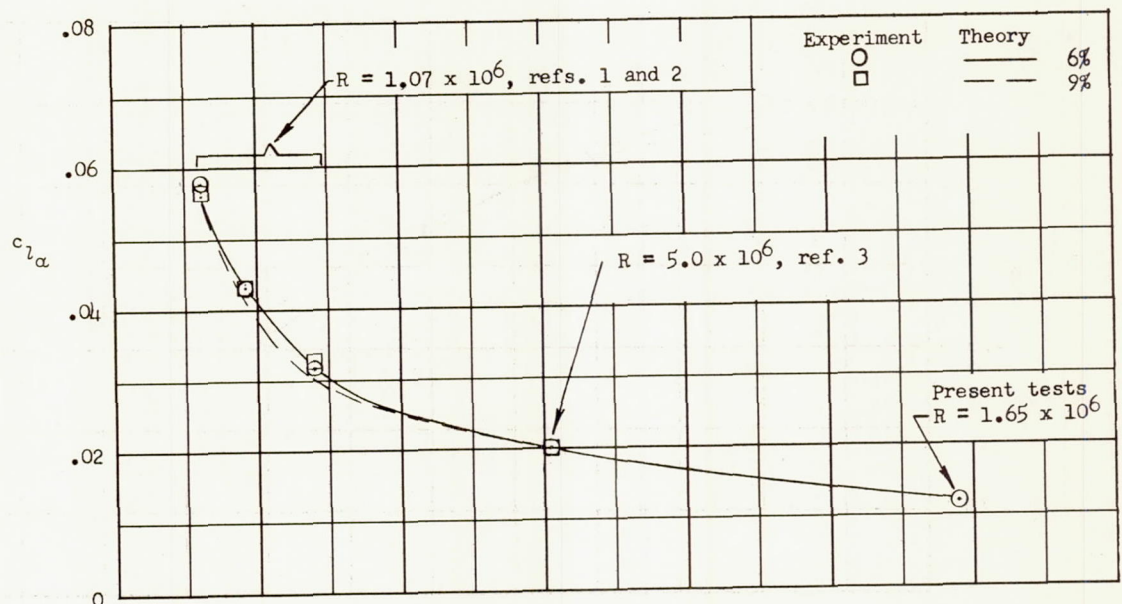


Figure 16.- The variation of slope parameters and pressure drag coefficient with Mach number for 6-percent-thick and 9-percent-thick symmetrical circular-arc airfoils with a 30-percent-chord trailing-edge flap. $\alpha = 0^\circ$; $\delta = 0^\circ$.

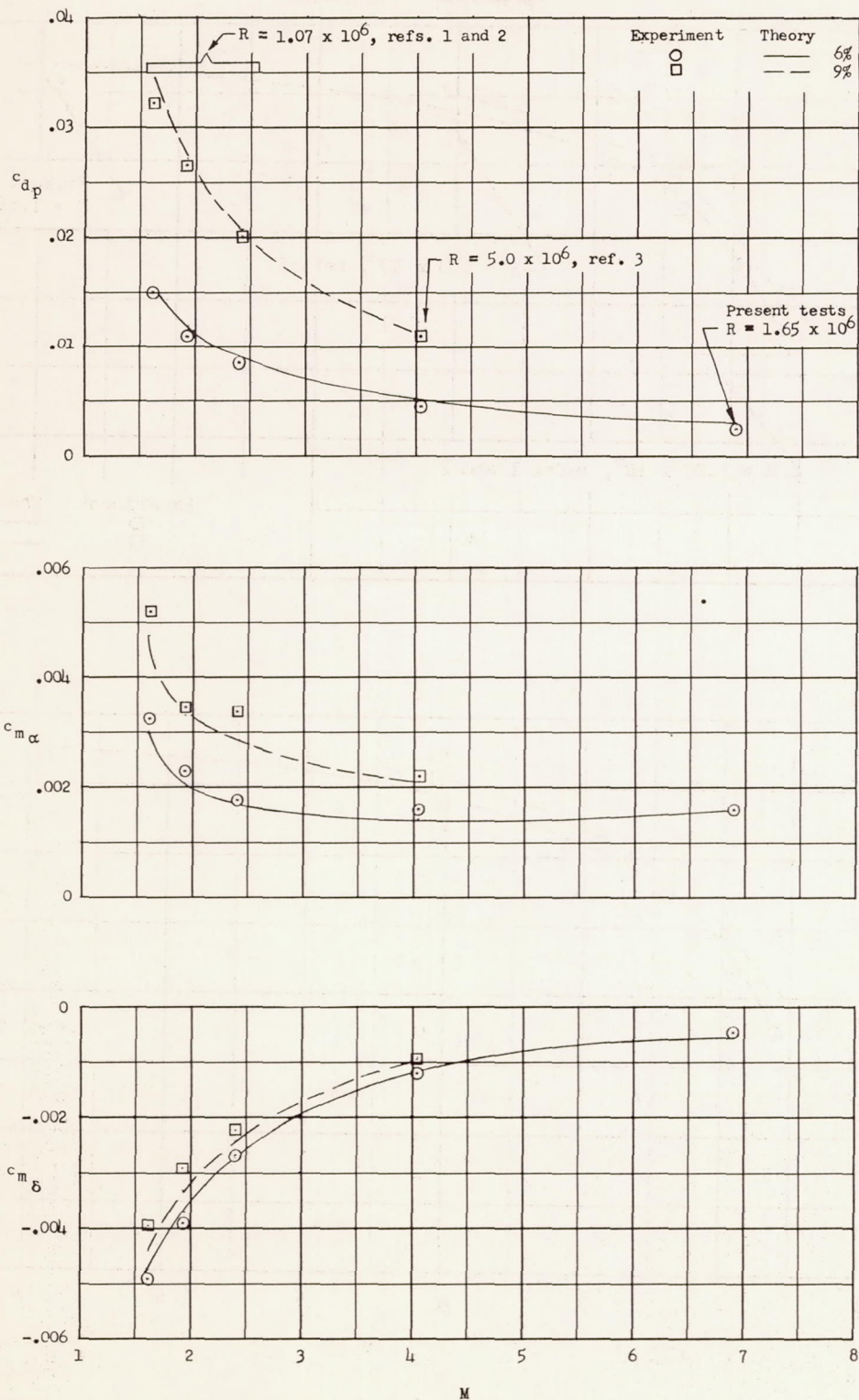


Figure 16.- Continued.

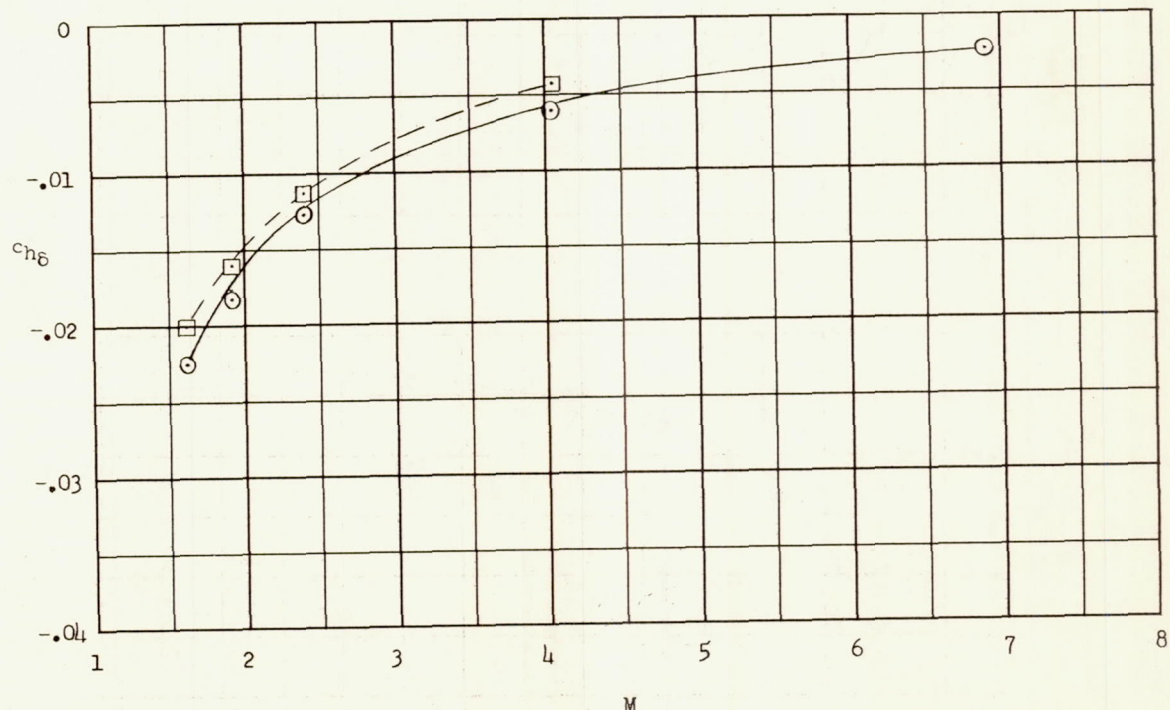
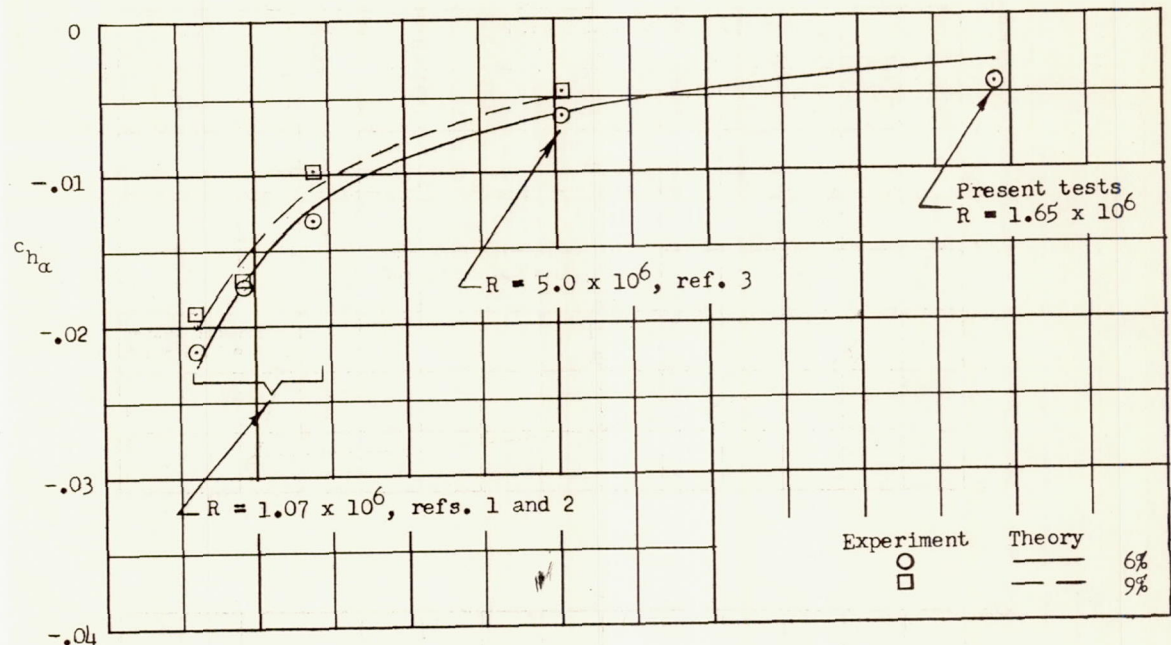


Figure 16.- Concluded.

CONFIDENTIAL

CONFIDENTIAL